International Journal of Mechanical and Thermal Engineering

E-ISSN: 2707-8051
P-ISSN: 2707-8043
IJMTE 2025; 6(1): 53-73
www.mechanicaljournals.com/ijmte
Received: 07-01-2025
Accepted: 09-02-2025

Kays A Al-Tae'y
Assistant Professor,
Engineering Collage,
University of Samarra, Iraq

Corresponding Author:
Kays A Al-Tae'y
Assistant Professor,
Engineering Collage,
University of Samarra, Iraq

Numerical simulation of vibration influence on the thermal periodic flow structure of liquid metal gallium in the enclosure with uniform internal heat generation

Kays A Al-Tae'y

DOI: https://www.doi.org/10.22271/27078043.2025.v6.i1a.77

Abstract
The natural convection heat transfer system in nuclear reactor systems may be subject to several external sources such as vibration. Thus, the natural convection due to buoyant force results from the interaction of density gradients with the acceleration field. In the present study, the numerical investigation of periodic oscillation thermal natural convection of a liquid metal gallium inside the internally uniform heated square enclosure. The enclosure is subjected to a sinusoidal oscillation vibration at low frequency. A time dependent governing equations were solved using a finite volume method based on a pressure-correction equation of the unsteady SIMPLE algorithm technique, and a collocated arrangement for scalar and vector variables in a non-uniform grid system. The top and bottom walls of the two-dimensional enclosure were isolated, whereas the side walls were isothermal cooled. The numerical simulations were performed on two case problems*:* uniform vibration amplitude at a constant frequency, and nonuniform vibration amplitude at a constant frequency. The results obtained for the internal Rayleigh number were 10^6. The results show that when the uniform vibration amplitude was increased from 0.01 mm to 100 mm at a frequency value equal to 1 Hz the natural periodic oscillation flow transitioned to a quasi-periodic flow. When uniform vibration amplitude values at 0.01 mm and 1.0 mm with frequency value 1 Hz, the time series at a certain time value appeared a sudden fall in counterclockwise streamfunction value and an unanticipated jump in clockwise streamfunction value. The result also indicates a rapid change in counterclockwise and clockwise streamfunctions values when the nonuniform vibration was applied with two different amplitude values in a sequential pattern at a certain frequency value. Therefore, the vibrations distort the original velocity and temperature field for oscillation thermal natural convection and new distributions appear, even at low vibration frequency and amplitude. The results showed that the heat transfer rate of thermal flow in the enclosure is proportional to vibration frequency and amplitude.

Keywords: Natural convection, square enclosure, liquid metal, heat generation, vibration

Introduction
A phenomenon of natural convection heat transfer due to internal heat generation with liquid metal occurs in many significant engineering applications; for example, cooling of nuclear reactor systems or heat removal from nuclear reactors. In a nuclear reactor, the core consists of fuel elements where the fission reaction proceeds. The energy released due to fission in the fuel element of a nuclear reactor ultimately appears in the form of heat and effect in increasing the temperature of the fuel element [1]. The heat is generated by the fissions, transferred from fuel elements by heat conduction to the surface of the fuel rod and through the cladding. From the surface of the cladding, the heat is transferred by convection to the coolant, which passes from the core to the external heat exchangers in which steam is generated to operate on a power cycle [2]. The reactors' thermal and hydrodynamic project aims to safely remove the heat without producing an excessive temperature in the fuels [3]. Hence, understanding the behaviour of internal heat generation in nuclear reactors is important. Possible heat generation effects may alter the temperature distribution and consequently the particle deposition rate in nuclear reactors [4]. The natural convection velocities and local flow directions depend on the temperature distribution of the coolant [5]. The nuclear reactor system which has a passive safety system that relies on a natural convection passive cooling system can remove the decay heat, by natural circulation, without the need for either an external power supply or an active system, which is strongly recommended for the next advance nuclear power plant [6].
The natural convection system in nuclear reactor systems may be exposed to external forces

such as mechanical vibration. The natural convection process from the heat-generating device is driven by buoyancy forces, which result from density gradient and gravity field. When a system with density gradients is subject to mechanical vibrations, the resulting buoyancy forces produced by the interaction of the density gradients with the acceleration field have a complex spatial and temporal structure that depends on both the nature of the density gradients and the spatial frequency distribution of the vibration-induced acceleration field [7]. The vibration behaviour affects a thermo-fluid system for increasing or decreasing the convective heat transfer, due to introducing the fluctuation and significant perturbations in the effective gravity, which change the flow patterns and lead to the oscillations of temperature distribution. Accordingly, the vibration that works like a gravitational field, can introduce periodic buoyancy flow. This is the so-called thermovibration effect [8].

In recent years, the case of natural convection heat transfers in an enclosure, when the flow is driven by a temperature gradient and imposed on a time-varying external force, has attracted much attention in many heat transfer analyses.

The numerical study for suppressing the natural convection of vertical zone-molting crystal growth by mechanical axial vibration was carried out by Lan [8]. The effect of applied vibration was incorporated into the gravitation acceleration. The simulation results showed that an axial vibration at a high frequency can affect the melt flow and the growth interface, whereas concave growth front due to buoyancy convection can be inverted easily to a convex one. However, at a low frequency of axial vibration, the model starts to break down and the resonance appears at about 0.5 Hz, where the flow oscillation and severe periodic growth and re-melting can be induced.

Kim *et al*. [9] experimentally studied a resonant phenomenon of natural convection in a side-heated cubic enclosure with a mechanically oscillating bottom wall. The two cases of Rayleigh number 7.3×10^7 and 1.2×10^8 were considered, and the oscillation frequency and amplitude of the bottom wall were varied between $356 < \omega < 8556$ and $0.03 < A < 0.06$, respectively. They observed that at a resonance frequency, the fluctuating amplitude of air temperature inside the enclosure showed a peak. Also, the resonant frequency increases with the Rayleigh number increase, however, it was little affected by increases in the oscillating amplitude of the bottom wall.

The nature of entropy generation for natural convection in a two-dimensional square enclosure filled with porous media and vibrating sinusoidal perpendicular to the applied temperature gradient and parallel to the vertical axis in a field of zero-gravity was numerically investigated by Mahmud and Fraser [10]. It concluded, that the gravity oscillation introduces a true periodic behaviour to the entropy number, Bejan number, and Nusselt number. They found that at the lower extreme of the gravity oscillation, the Nusselt number and entropy number are minimum and the Bejan number is maximum, but at the upper extreme of the gravity oscillation the Bejan number is minimum and the Nusselt number and entropy number are maximum.

A numerical analysis of the natural convection heat transfer in a differentially heated enclosure was done by Jalil and Al-Tae'y [11] to evaluate the effect of magnetic field application on the heat transfer coefficient within a fluid-filled two-dimensional square enclosure. The enclosure is subject to vertical mechanical vibration. The results are presented in terms of Prandtl number = 0.71, Rayleigh number = 10^4, and vibration Grashof number = 10^6 with different values of Hartmann number and angular frequency of vibration. Moreover, results it was concluded that the application of a magnetic field can be abatable the non-uniform behavior of Nusselt number oscillation due to vibration and generates a uniform oscillation, and the amplitude of frequency decreases with an increase in magnetic field strength and thus causes a decrease in Nusselt number value.

The effect of thermovibration on convection structure and instability in Marangoni-Benard convection and Rayleigh-Marangoni-Benard convection in a two-layer liquid system heated from below has been numerically studied by Liu *et al*. [12]. The fluid upper is Silicone oil and Flour inert is the fluid bottom. The temperature gradient is imposed perpendicular to the interface of the fluids. The interfacial tension at the interface is assumed to be a linear function of temperature. The linear instability analysis results show that the thermovibration similarly affects the Marangoni-Benard convection and Rayleigh-Marangoni-Benard convection. It found the vibrations with the vertical direction to the interface can enhance the stability of the two-layer system and dampen the convective flow down. However, horizontal vibrations strengthen the system's instability and make it apt to lose its stability.

Shevtsova *et al*. [13] investigated experimentally the effect of vibrations for induced convection in a cubic cavity that was heated and cooled from above and bottom walls, respectively, with microgravity conditions of a parabolic flight. The temperature gradient was opposed to the gravity vector and the frequency and amplitude of vibration varied in ranges of 1 - 2 Hz and 10 - 140 mm, respectively. They experimented with three conditions; microgravity and no vibrations, microgravity and vibrations, and normal gravity and vibrations. It demonstrated the strong heat transport to the mean flow under

the vibration in low gravity. This transport is weaker in the absence of vibration and negligibly small in normal gravity.

A numerical simulation of vibration-induced mixed convection in an open-ended cavity filled with a porous obstructed medium has been investigated by Chung and Vafai [14]. The left wall vibrates vertically and parallel to gravity acceleration. It is shown that increasing the vibrational Reynolds number and/or Darcy number enhances the vibrational effect, and high values of vibrational Reynolds number lead to the formation of a vortex. They found an increase in vibrational Reynolds number and/or modified Rayleigh number resulting in an enhancement in heat transfer. Also, they found that as the obstructing medium becomes more permeable and at larger values of vibrational Reynolds number, the vibrational effect becomes more substantial and leads to the formation of a vortex at the left corner of the cavity.

Aktas [15] investigated numerically the effect of the oscillatory flow of nanofluid on convective heat transfer in a rectangular shallow pressurized enclosure at 5 bar filled with water-γAl_2O_3. The vertical and horizontal walls of the enclosure are adiabatic and heated differentially, respectively. The periodic vibration of the left adiabatic wall of the enclosure drove the nanofluid motion. It evaluated the effect of left wall displacement amplitude at 20 nm and 25 nm, particle volume concentration at 0.01 and 0.05, and

horizontal walls temperature difference at 0.1 K and 0.2 K on the transient thermal convection in the enclosure. It observed that the oscillatory flow significantly augments the heat transfer when compared to pure conduction and the augmentation is more evident at low nanoparticle volume concentration.

A mathematical simulation model for the effect of mechanical vibration on melt hydrodynamics and crystal structure formation during directional solidification was performed by Fedorov *et al*. [16]. Crystal growth by the Bridgman method and floating zone method under terrestrial conditions and in microgravity with vibrations imposed on the melt. Vibrations occur along the crystal axis and are harmonic. It was shown that the application of low frequency and small amplitude of vibrations (vibration acceleration lesser than 10^{-2} m/sec^2) may cause suppression of secondary vortex flows in both crystal growth methods. Alternating low-frequency vibrations, (vibration acceleration larger than 10^{-2} m/sec^2) may induce Rayleigh-Taylor instability of the melt flow in the Bridgman method, but at the same conditions, the floating zone method characterized by a stable melt flow, and vibrations lead only to the change in the melt flow direction.

An experimental investigation was carried out by Wang *et al*. [17] to find the effect of vibration on heat transfer performance for a pair of cold and hot horizontal microtubes staggered in a relatively large concentric horizontal adiabatic cylindrical enclosure. It shows that when the vibrational disturbance is weak, the relative effect of vibration on a given natural convection is weakened, and when the vibrational disturbance is strong the relative effect is strengthened as well, the best vibration strength ratio effect is about 6.16.

Xie and Cao [18] analyzed the effects of wall vibrations on the natural convection of non-Newtonian power-law fluids in a rectangular cavity. It has been analyzed within the framework of the Boltzmann lattice method. The longitudinal and transverse vibrations are applied to the horizontal walls of the cavity separately, and the two vertical walls are differentially heated. The effects of the power-law index in the range of 0.5 - 1.2 on momentum transport and heat transfer are investigated for the Rayleigh number in the range of 10^3 - 10^5 and the Prandtl number of 10. The average Nusselt number was smaller under wall vibrations than that without wall vibrations. At low Rayleigh numbers, wall vibrations showed slight or no influence on the averaged Nusselt number of power-law fluids. The effects of wall vibrations on the streamlines, isotherm contours, and heat transfer characteristics of power-law fluids have been observed obviously at a high Rayleigh number.

Crewdson and Lappa [19] have investigated a numerical simultaneous effect of vibrations on the natural convection of a liquid in a two-dimensional square cavity. The vibrations and temperature gradient are parallel, and microgravity conditions are assumed. A fluid with a Prandtl number 15 and a vibrational Rayleigh number spans the interval from 10^4 to 10^6. In addition, they concentrated on the effective patterning behaviour of the flow for the different regimes where clusters of convective modes can be observed as a function of values of vibrational Rayleigh number, i.e., stable state, the synchronous and periodic state, subharmonic state, synchronous and non-periodic state, and non-synchronous and non-periodic state. They found that for all values of the Rayleigh vibrational number, at low frequencies, the maximum Nusselt number remains constant; it grows for medium frequencies and finally decreases for high values of frequencies.

An experimental study was performed by Kays *et al*. [20] for the effect of pulsate surface heat flux on the single-phase buoyancy driven convection of ethylene glycol flow through a minichannels heat sink. Four heat flux frequencies are used with a constant amplitude, Rayleigh number, and duty cycle. It was observed that for the complete power cycle through the loop thermosyphon and at high heat flux frequency, there is insufficient time for on-cycle conditions to exist in the channel. Thus, a small amount of heat is delivered to the fluid through the minichannel wall to increase its temperature. At low operation frequency, the outlet fluid temperature and the heater wall temperature increase due to the high residence time of the power supply during on-cycle. The oscillation of the outlet fluid temperature causes the oscillation of the inlet fluid temperature to the minichannel.

A literature survey shows that vibration is important for engineering applications in bouncy-driven natural convection systems. The main intent of this study is to investigate numerical simulations of the interaction of vibration in sinusoidal modulations with periodic oscillation natural convection of liquid metal gallium in the enclosure. The thermo-fluid system is subjected to vibration, which is parallel to the direction of gravity acceleration, so the fluid flow domain in the square enclosure is subject to two components; the static gravity, *g*, and the oscillatory acceleration component or time-dependent accelerations, *g*-jitter. The objectives of the current study are to investigate the influence of the sinusoidal vibration modulations with (a) uniform vibration amplitude, and (b) nonuniform vibration amplitude by taking two different values of amplitude which are effective in a sequential pattern.

2. Physical System Model and Mathematical Formulation

A typical molten gallium, Pr = 0.024, filled two-dimensional square enclosure of height H and width L is shown in Fig. 1. The left and right solid walls are at a constant temperature, and the upper and lower solid walls are insulated, the wall is considered to be plane. The fluid is motioned by uniform internal heating. The Boussinesq approximation is invoked for the fluid properties to relate density changes to temperature change. The enclosure is subjected to a vibration effect due to an oscillatory acceleration component called a *g*-jitter. The enclosure vibration is modelled by a harmonic contribution to the body force. The static gravity, *g*, and the oscillatory acceleration component, *g*-jitter, are assumed to be perpendicular to the thermal gradient.

The thermo-flow considers the unsteady two-dimensional periodic oscillatory natural convection flow of a Newtonian and incompressible fluid. Under these assumptions, the conservation equation for mass, momentum, and energy at each point in a two-dimensional Cartesian coordinate system are as follows [21]:

The principle of mass conservation applied to the thermo-fluid for the variation of the density results in the following equation:

$$\frac{\partial \rho}{\partial t} + \frac{\partial}{\partial x}\rho u + \frac{\partial}{\partial y}\rho v = 0 \quad (1)$$

The principle of momentum conservation was represented by the Navier-Stokes equations. In the *x*-direction, this equation writes

$$\frac{\partial}{\partial t}\rho u + \frac{\partial}{\partial x}\rho uu + \frac{\partial}{\partial y}\rho vu = -\frac{\partial p}{\partial x} + \frac{\partial}{\partial x}\left(\mu \frac{\partial u}{\partial x}\right) + \frac{\partial}{\partial y}\left(\mu \frac{\partial u}{\partial y}\right) \quad (2)$$

whereas in the *y*-direction, the equation is

$$\frac{\partial}{\partial t}\rho u + \frac{\partial}{\partial x}\rho uu + \frac{\partial}{\partial y}\rho vu = -\frac{\partial p}{\partial x} + \frac{\partial}{\partial x}\left(\mu \frac{\partial u}{\partial x}\right) + \frac{\partial}{\partial y}\left(\mu \frac{\partial u}{\partial y}\right) \quad (2)$$

$$\frac{\partial}{\partial t}\rho v + \frac{\partial}{\partial x}\rho uv + \frac{\partial}{\partial y}\rho vv = -\frac{\partial p}{\partial y} + \frac{\partial}{\partial x}\left(\mu \frac{\partial v}{\partial x}\right) + \frac{\partial}{\partial y}\left(\mu \frac{\partial v}{\partial y}\right) + \rho\beta(T - T_c)[g + b\omega^2 \sin\omega t] \quad (3)$$

By assuming there is no-viscous dissipation term and with uniform internal heat generation and heat-induced by viscous dissipation due to an oscillating liquid metal thermal flow is negligible. The principle of conservation of energy is expressed by the following equation:

$$\frac{\partial}{\partial t}\rho T + \frac{\partial}{\partial x}\rho uT + \frac{\partial}{\partial y}\rho vT = \frac{\partial}{\partial x}\left(\frac{\mu}{Pr}\frac{\partial T}{\partial x}\right) + \frac{\partial}{\partial y}\left(\frac{\mu}{Pr}\frac{\partial T}{\partial y}\right) + \frac{Q}{Cp} \quad (4)$$

The rigid sidewalls are impermeable and no-slip boundary conditions are imposed at all boundaries. The hydraulic and thermal imposed boundary conditions are shown in the physical system model, see Fig. 1, and are written mathematically as form:

$t > 0$	$x = 0, L$	$u = v = 0$	$T = T_c$	$0 < y < H$
$t > 0$	$y = 0, H$	$u = v = 0$	$\partial T/\partial y = 0$	$0 \le x \le L$

For the initial conditions at $t = 0$ sec, the velocities in the computational domain are set equal to zero and the initial field temperature is equal to cold wall temperature T_c with a uniform internal volumetric heat generation Q.

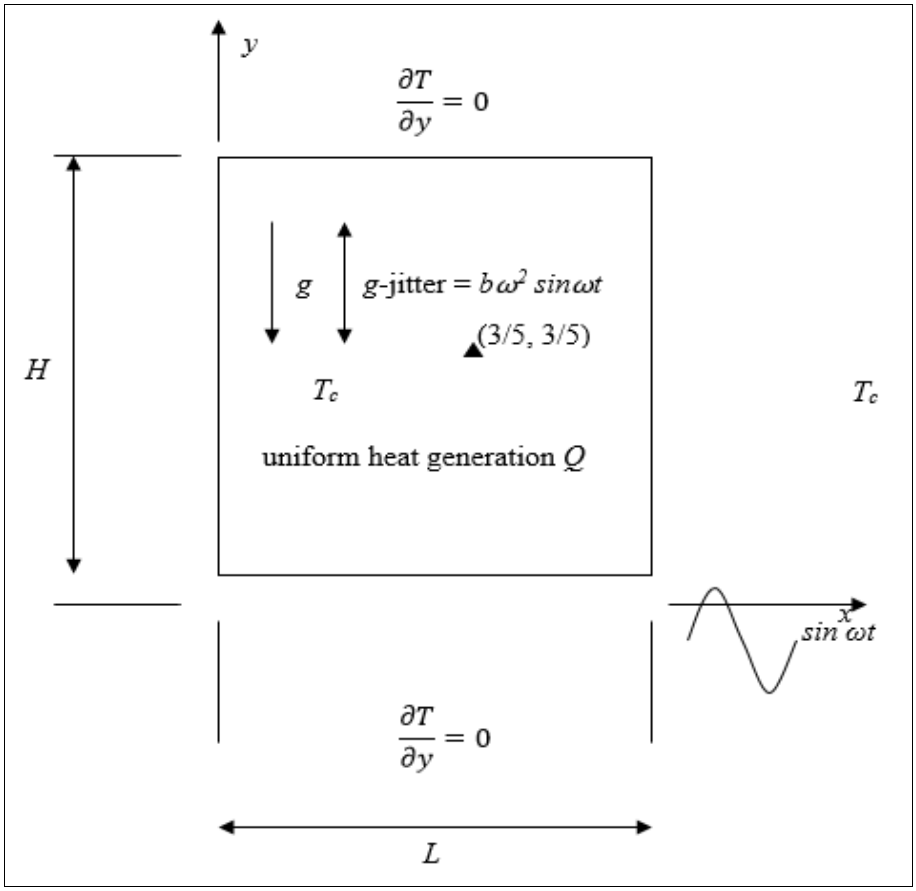

The fluid motion is displayed using the streamfunction, which is obtained from velocity components [22]. The relationships between streamfunction and velocity components for two-dimensional flows are:

$$u = \frac{\partial \psi}{\partial y} \quad (5)$$

$$v = -\frac{\partial \psi}{\partial x} \quad (6)$$

Which yield a single equation of the streamfunction

$$\frac{\partial^2 \psi}{\partial x^2} + \frac{\partial^2 \psi}{\partial y^2} = \frac{\partial u}{\partial y} - \frac{\partial v}{\partial x} \quad (7)$$

The no-slip condition is valid at all boundaries as there is no cross-flow, hence

$t > 0$	$x = 0, L$	$\psi = 0$	$0 < y < H$
$t > 0$	$y = 0, H$	$\psi = 0$	$0 \le x \le L$

The heat transfer rate across the fluid layer be expressed in terms of a local Nusselt number at the cold walls defined as

$$Nu_y = \frac{\partial T}{\partial x}\frac{H}{T_{max}} \quad (8)$$

The average Nusselt number is calculated by integrating the local Nusselt number along the vertical wall

$$Nu = \frac{1}{H}\int_0^H Nu_y\, dy \quad (9)$$

3. Computational Methods

The governing two-dimensional transient incompressible thermo-fluid flow equations and the boundary conditions are discretized via the finite volume technique. The pressure-correction equation of the SIMPLE-method and a collocated arrangement for scalar and vector variables are used; see Ferziger and Perić [23]. The PCOL package is used to solve the algebraic system of equations in velocity, pressure, and temperature. It is set for buoyancy-driven flow in the closed enclosure and solved within an iterative sequence. The three-time level scheme is used for the transient terms and the central difference scheme for the convection terms and the diffusion terms.

3.1. Computational grid

Grid independence tests have been performed as described by Al-Tae'y [24] and Jalil *et al.* [25], which conducted for the present problem, and results are shown in Figs. 2 and 3. The maximum deviation in the average Nusselt number value of the selected grid (x,y) = 132 × 132 relatives to the other grids are plotted as functions of several grid points. Including results for six grids ranging (x,y) from 100 × 100, 116 × 116, 126 × 126, 132 × 132, 140 × 140, and 148 × 148 nodes. The flow was time-dependent at Pr = 0.024 and $Ra_I = 10^6$. It found that maximum deviation at t = 30 sec for the two meshes 132 × 132 and 148 × 148 are less than 1.7% at x = 0 and 2.2% at $x = L$ as illustrated in Fig. 2 (a) and (b), respectively. Also, the maximum temperature variation of the selected grid (x,y) = 132 × 132 relative to 148 × 148 at t = 30 sec is less than 1.06% as illustrated in Fig. 3. From these results and by considering the accuracy and the computational cost a grid with 132 × 132 used.

The construct of a non-uniform collocated grid system with finer grids is concentrated in the region of all the wall boundaries in which the grid expands at constant rates from the walls to the interior region of the enclosure. It's expected that the non-uniform grids give a more accurate result than uniform grids [23].

The time-step size of Δt is 0.01 sec considered sufficiently small to render the solution insensitive to time-step size.

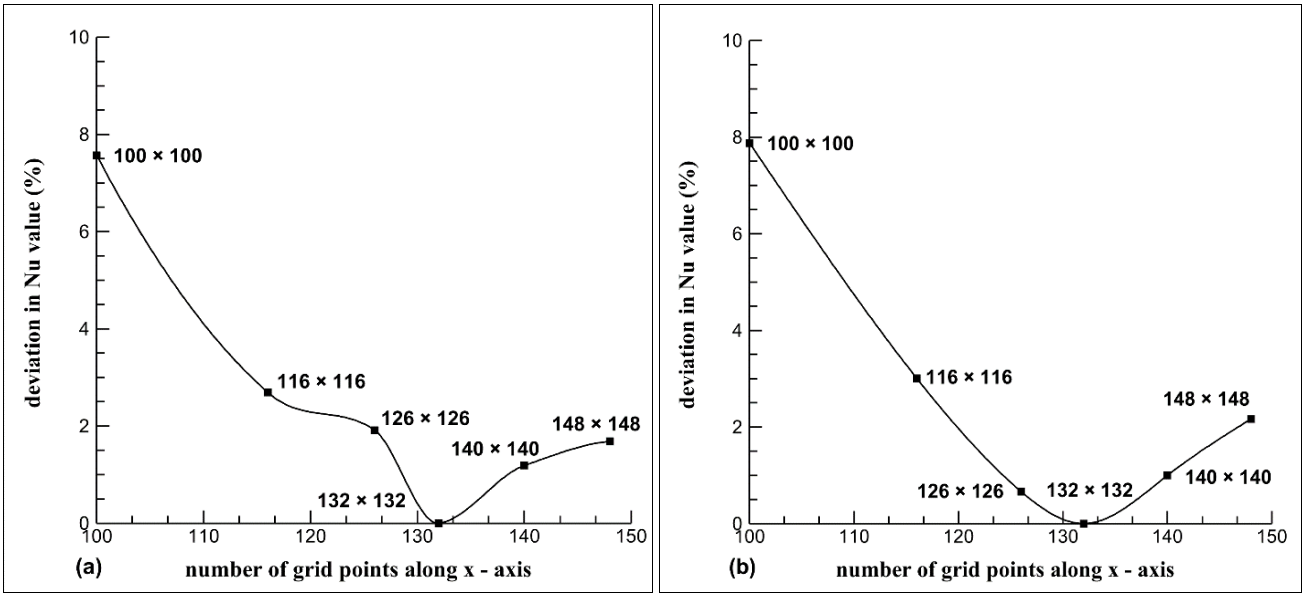

Fig 2: The maximum deviation in average Nusselt number value of the selected grid (x,y) = 132 × 132 relative to the other grids for Pr = 0.024, $Ra_I = 10^6$ and t = 30 sec: (a) deviation in average Nusselt number value at x = 0; (b) deviation in average Nusselt number value at $x = L$.

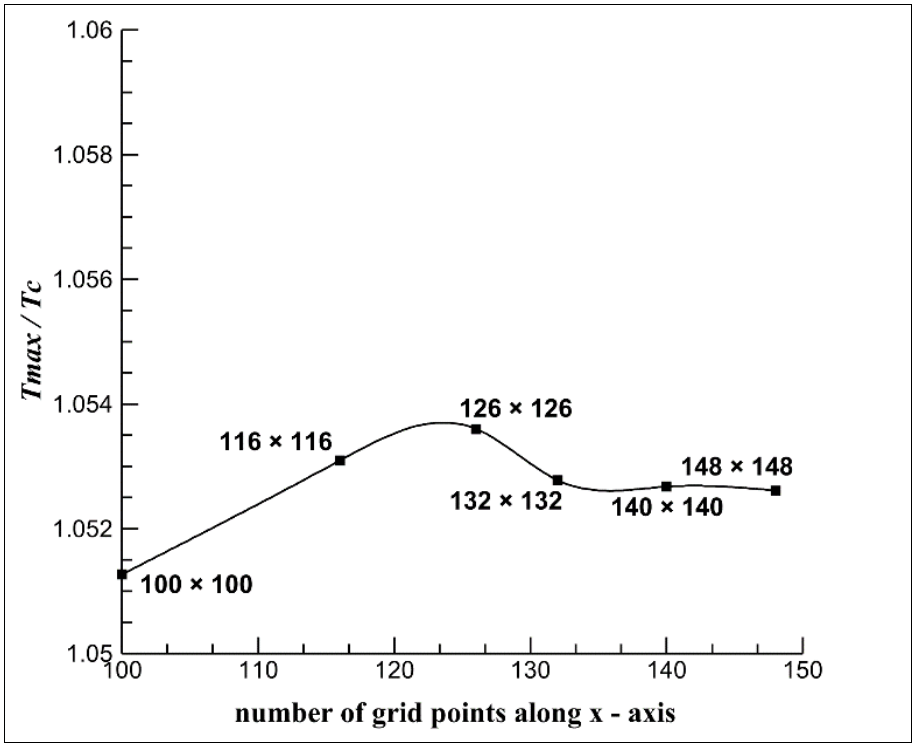

Fig 3: Time-average maximum temperature variation of the selected grid (x,y) = 132 × 132 relative to the other grids for Pr = 0.024, Ra_I = 10^6 and t = 30 sec.

3.2. Numerical methods validation

The numerical program used in this study has been also used by Al-Tae'y [24] to illustrate the effect of time-periodic boundary conditions on natural convection in an enclosure. In addition, Jalil *et al.* [25] used this numerical program to investigate the natural convection in an enclosure with a magnetic field effect. This numerical program was validated by using numerical solutions of other previous studies [24, 25]. The performance of the present numerical analysis, which is employed to solve the present problem considered in this study, will be checked by calculate the average Nusselt number for the case of two-dimensional steady state natural convection in a square enclosure. The enclosure is differentially heated vertical walls and insulated horizontal walls and filled with liquid metal gallium. The numerical results were compared with the results of the average Nusselt number reported by Viskanta *et al.* [26], as presented in Table 1. The mesh used to predict the detailed flow structure for low-Prandtl number fluids by Viskanta *et al.* [26] is (x,y) = 41 × 41 and a mesh use in the present study is (x,y) = 50 × 50, 50 × 50, 42 × 42, and 44 × 44 for Ra = 10^4, 10^5, 10^6, and 10^7, respectively. The deviation between the reported results and obtained results may be due to the solution techniques, the computational schemes used [27], and grid points.

Table 1: The comparison of the average Nusselt number of the present study with that given by Viskanta *et al.* [26].

Pr / Ra	**10^4**	**10^5**	**10^6**	**10^7**	
0.01	1.571	2.975	6.121	13.327	Viskanta study [26]
0.02	1.765	3.257	6.701	15.120	Viskanta study [26]
0.05	1.978	3.657	7.160	16.936	Viskanta study [26]
0.024	0.858	1.562	3.033	6.132	Present study (steady state)

4. Results and Discussion

This research studies the effect of sinusoidal oscillation vibration on the periodic oscillation natural convection mode in a square enclosure. The effect of vibration is along the static gravity direction. The Prandtl number used in the present numerical calculation is 0.024 which is the value corresponding to molten gallium. The periodic thermal flow regime in the enclosure is established for the value of the internal Rayleigh number is 10^6. In the parametric study, only one parameter is varied, amplitude or frequency of vibration, while the others are kept constant and the values of other parameters are initiated at first.

The flow field, the temperature gradients, and Nusselt number inside the enclosure are presented to illustrate the effect of amplitude and frequency of vibration.

4.1. The effect of uniform vibration amplitude at a constant vibration frequency

When only static gravity exists: initially at t = 0 sec the left and right walls are cold and there is no fluid motion inside the enclosure. As heating starts, the fluid temperatures rise. The molten gallium moves are driven by a buoyancy force generated by a temperature gradient in an enclosure. The construction of the flow at the time becomes 900 sec is illustrated by the maps of streamfunctions and isotherms in Fig. 4(a) and (b). As a result, the main two-vortices structure with opposite rotating directions and anti-symmetric concerning reflection plane x = ½ L are formed in flow regions. The regime of the isotherms is denser on the top part of the cooled two-vertical walls these indicate that heat transfer through these parts of the walls is greater.

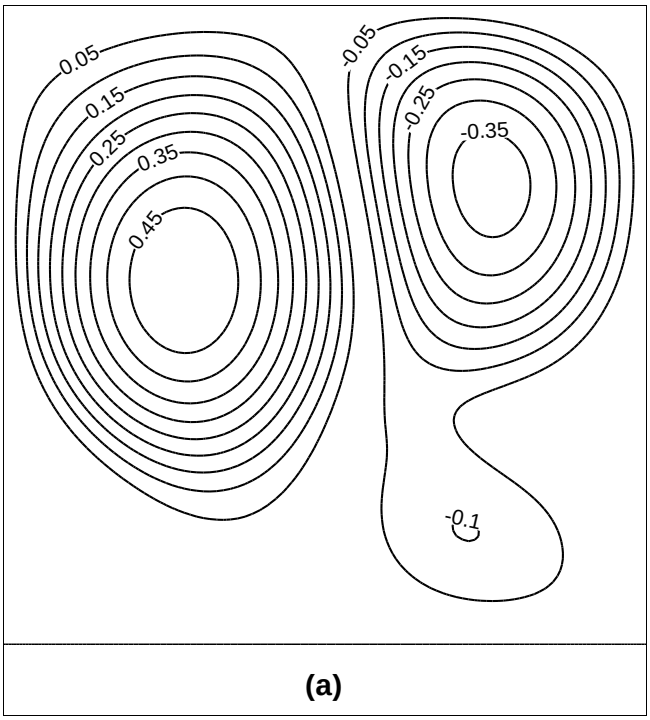
-0.05
-0.15
-0.25
-0.35
-0.1
0.05
0.15
0.25
0.35
0.45

(a)

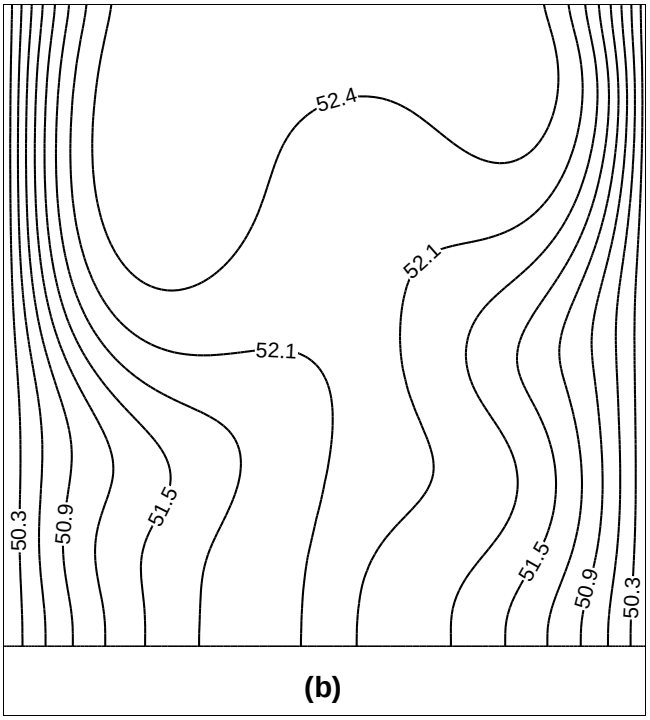
52.4
52.1
52.1
50.3
50.9
51.5
51.5
50.9
50.3

(b)

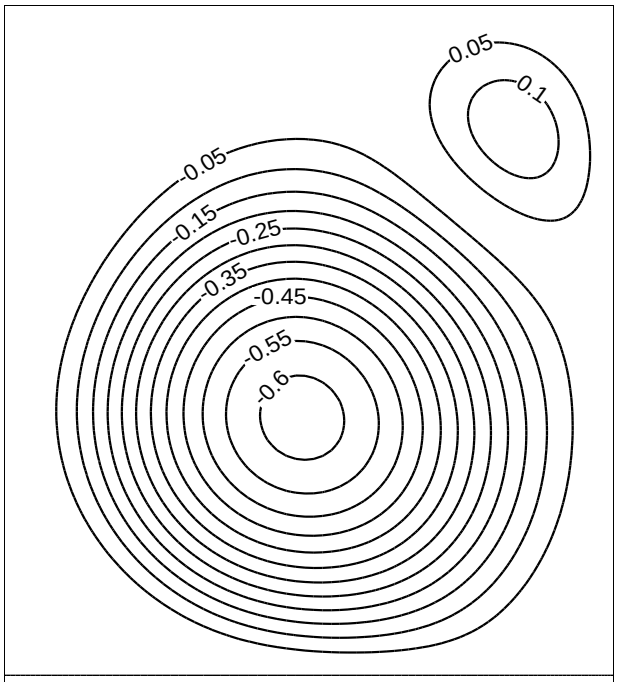
0.05
0.1
-0.05
-0.15
-0.25
-0.35
-0.45
-0.55
-0.6

(c)

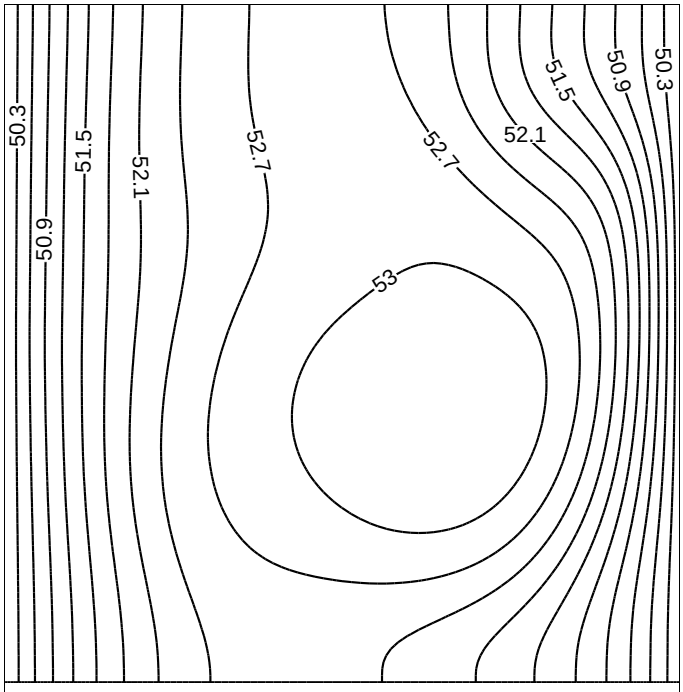
50.3
50.9
51.5
52.1
52.7
52.7
52.1
53
51.5
50.9
50.3

(d)

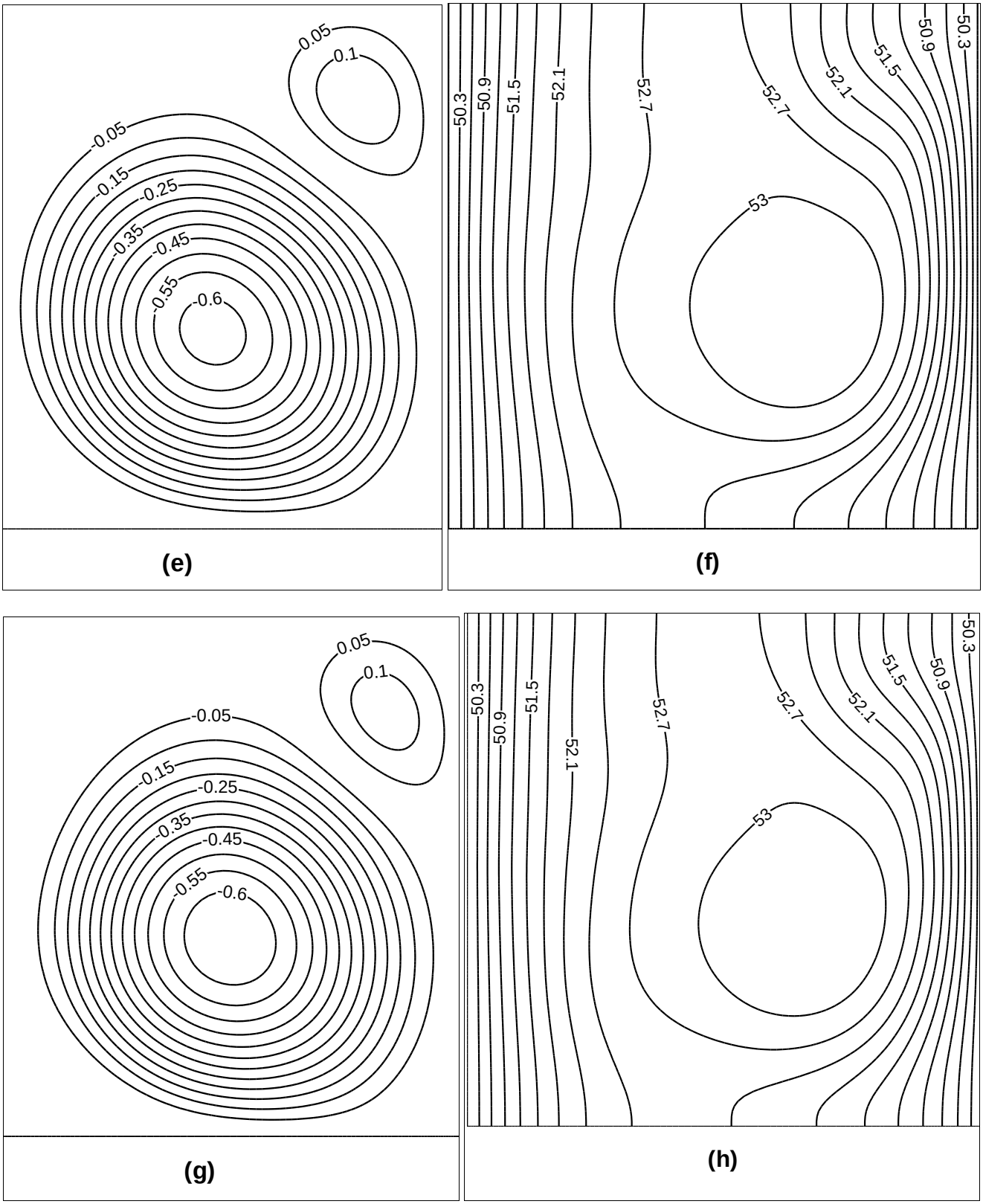

Fig 4: Streamfunctions (left) and isotherms (right) without and with thermovibration effect for Pr = 0.024, $Ra_I = 10^6$ and t = 900 sec. Thermovibration starts at t = 0 sec and stops at t = 900 sec: (a, b) without thermovibration effect; (c, d) with thermovibration effect at f = 1 Hz and b = 0.01 mm; (e, f) with thermovibration effect at f = 1 Hz and b = 1.0 mm; (g, h) with thermovibration effect at f = 1 Hz and b = 100 mm.

When the vibration frequency at f = 1 Hz and amplitude at b = 0.01 mm were applied, the redistribution of the thermal molten gallium in the enclosure appeared. The main and dominant vortex structure with clockwise circulation is presented and occupies the whole enclosure with a small secondary cell appearing in the upper right corner and it is rotating in the counterclockwise direction as illustrated in Fig. 4(c) at the time becomes 900 sec. The temperature inside the enclosure is dependent on the flow field and the isotherms are distorting as illustrated in Fig. 4(d).

In the case when the vibration frequency at f = 1 Hz and applied amplitude increase to b = 1.0 mm, the thermal

molten gallium flow and temperature distribution in an enclosure at the time t = 900 sec are illustrated in Fig. 4(e) and (f), respectively. The maps of streamlines and isotherms are similar to that at the state of vibration frequency at f = 1 Hz and applied amplitude b = 0.01 mm.

When the amplitude increases to b = 100 mm the vibration frequency is f = 1 Hz. The streamfunction and isotherms are shown in Fig. 4(g) and (h), respectively. As indicated by these figures and according to the streamlines, it can be observed dominant mono-cellular flow turns in the clockwise direction for all cases of thermovibration, whereas, a small counterclockwise rotating cell appears at the right top corner of the enclosure. The fluid flow in the enclosure is abnormal in its direction compared with the case without mechanical vibration effect as shown in Fig. 4(a) and (b). This is due to the effects of vibration that distorted the normal fluid flow direction and temperature distribution. The corresponding isotherms show the characteristics of conduction for dominated regimes except at the central part and right half of the enclosure because they are distributed approximately parallel to the active left wall.

The time series of maximum and minimum streamfunction without vibration effect is illustrated in Fig. 5(a). The flow field is laminar and initially transient until $t \approx 25$ sec, the destabilized flow with fluctuations is started to develop and results in regular periodic oscillations from $t \approx 25$ sec to $t \approx 45$ sec. The thermal convection flow becomes a periodic state with one fundamental frequency when $t > 45$ sec as shown in Fig. 5(b). This is according to hydrodynamic stability theory [18] which light fluid is below heavy fluid, and the density distribution could lead to instability and oscillation. The oscillatory behavior of the streamfunction variation is due to the unsteady interaction between flow cells [28].

The time series of maximum and minimum streamfunction at vibration frequency f = 1 Hz and amplitude b = 0.01 mm is illustrated in Fig. 5(c). The smooth and uniform curve appears until $t \approx 692$ sec this indicates the flow is laminar and non-oscillating with the light increasing the values of clockwise and counter-clockwise vortices. One can observe the vibration at a certain frequency and amplitude can destroy and dampen the natural periodic oscillation, because the vibration frequency is different from the natural frequency of flow oscillation. At $t > 692$ sec the flow becomes unstable, and fluctuating phenomena appear with a step-by-step increase in frequency and amplitude of flow. Then the sudden change happens in maximum and minimum streamfunction values until $t \approx 737$ sec as illustrated in Fig. 5(d). When $t > 737$ sec, the flow becomes stable and oscillates periodically. This anomaly is where the sudden fall in the maximum streamfunction value with a sudden jump in the minimum streamfunction value, and then the flow returns to its oscillation state that may be due to reverse flow. A reverse flow happens near the right vertically cooled wall by a small secondary cell appearing in the upper right corner of the enclosure and near the left vertically cooled wall by the main vortex as in Fig. 4(c). The wall boundary layers become unstable by reverse flow and interaction between the boundary layers and internal flow near the walls [29].

The time series of maximum and minimum streamfunction at vibration frequency f = 1 Hz and amplitude b = 1.0 mm are illustrated in Fig. 5(e). It is shown that after the time $t \approx$ 10 sec, the flow transitions to periodic flow with a very small amplitude until the unstable equilibrium point when the time $t \approx 705$ sec. At an unstable equilibrium point, the strength of the maximum streamfunction is decreasing and oscillates at a large amplitude of about the main value of 0.1288 m^2/sec, and the strength of the minimum streamfunction is increased and oscillates at a small amplitude of about the main value - 0.6171 m^2/sec. The oscillation trajectory for velocities is shown in Fig. 5(f), the flow is periodic and dependent on the superposition of vibration frequency and natural periodic oscillation frequency. In this flow regime, another frequency is added to the fundamental frequencies in Fig. 5(d) and the trajectory has a closed structure.

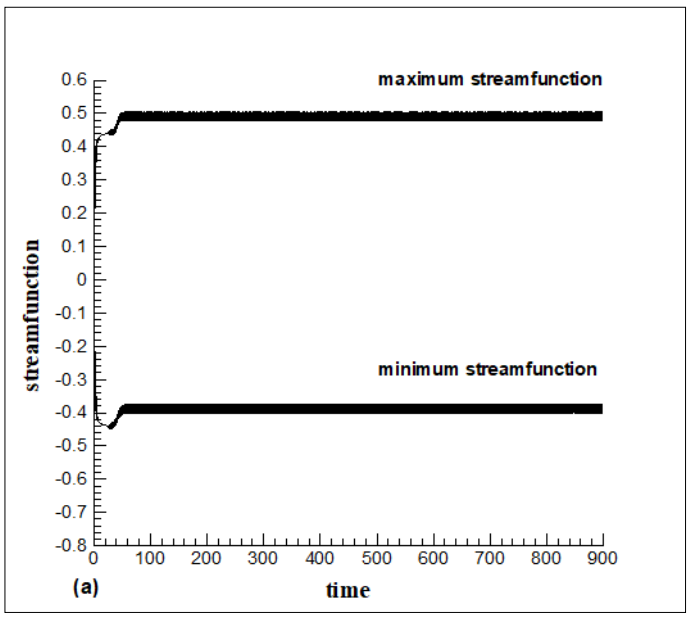

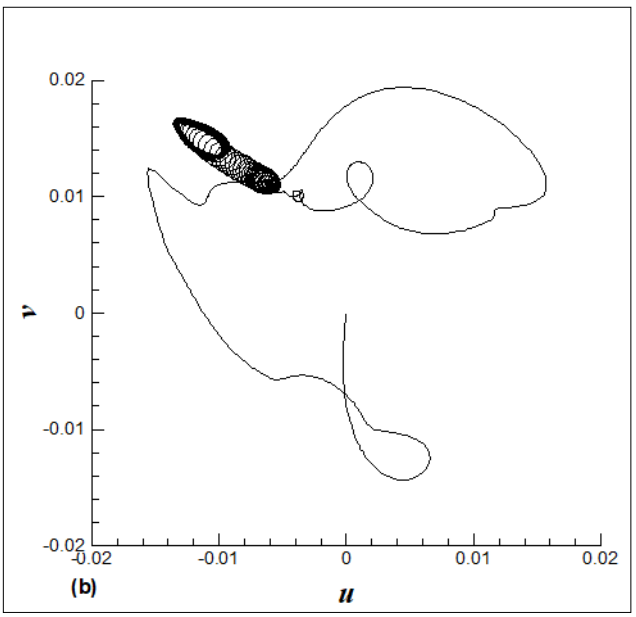

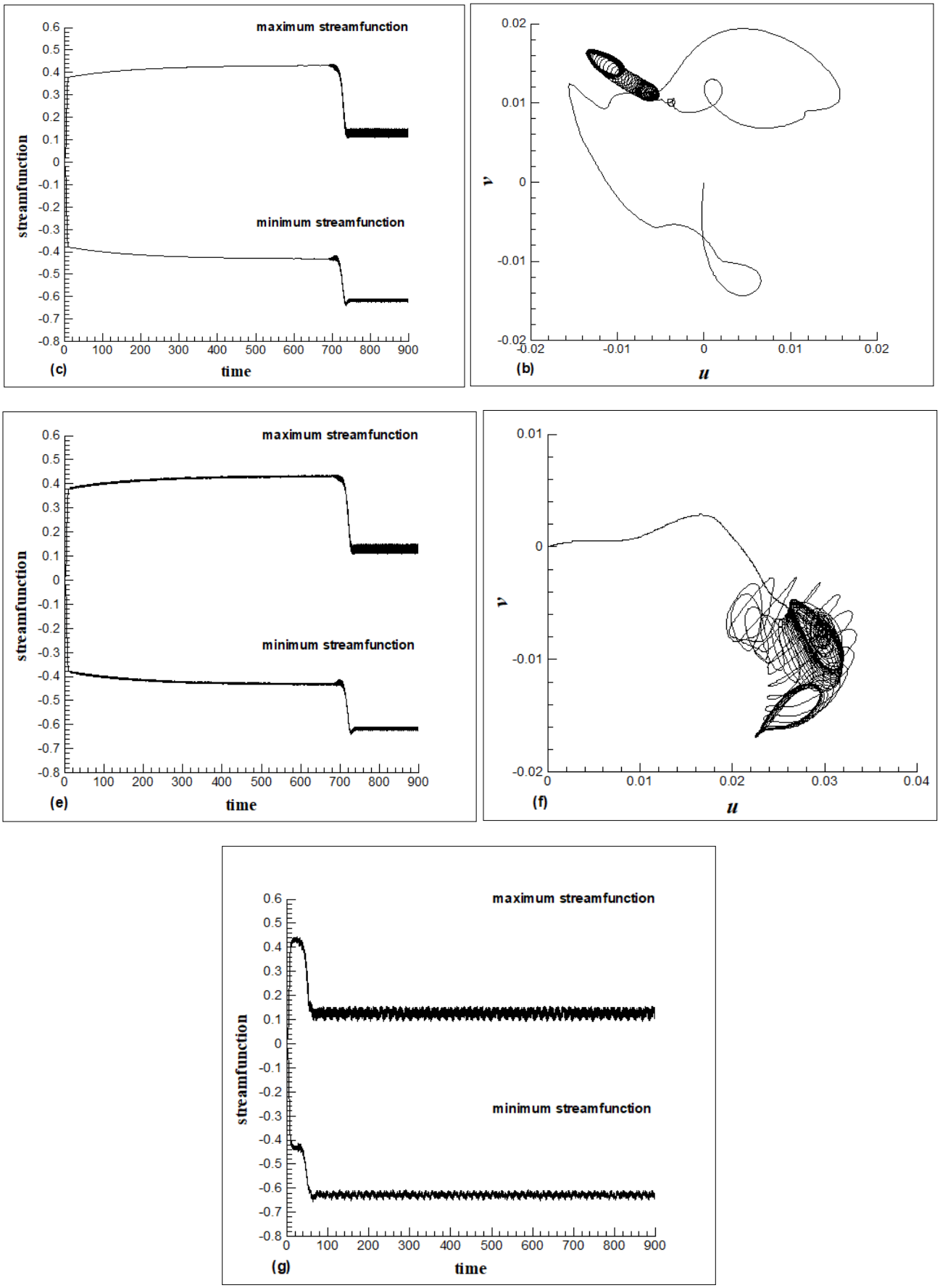

Fig 5: Time series of maximum (> 0) and minimum (< 0) streamfunction (left) oscillations and oscillation trajectory for *u*-velocity and *v*-velocity at $x = 3/5\ L$ and $y = 3/5$ (right) without and with thermovibration effect for $Pr = 0.024$, $Ra_I = 10^6$ and $t = 900$ sec. Thermovibration starts at $t = 0$ sec and stops at $t = 900$ sec: (a, b) without thermovibration effect; (c, d) with thermovibration effect at $f = 1$ Hz and $b = 0.01$ mm; (e, f) with thermovibration effect at $f = 1$ Hz and $b = 1.0$ mm; (g, h) with thermovibration effect at $f = 1$ Hz and $b = 100$ mm.

The time series of maximum and minimum streamfunction when the amplitude is increased to 100 mm at a vibration frequency of f = 1 Hz, as illustrated in Fig. 5(g). The fluid frequency increases gradually and the flow becomes markedly oscillatory with great amplitudes to become quasi-periodic. This means the transition from periodic flow to quasi-periodic flow occurs as the mechanical vibration amplitude increases. At b = 100 mm, the flow only takes about 8 sec to destabilize and oscillate periodically. The counterclockwise and clockwise vortex suddenly drop and jump around t = 8 sec, respectively, to a transitioning stage, and as time further proceeds about 55 sec the flow finally attains a quasi-periodic after t = 65 sec. The oscillation trajectory for velocities is shown in Fig. 5(h), the flow is quasi-periodic with multi-frequency and multi-amplitude values.

The variations of the characteristic of the fluid flow amplitude and frequency are associated with the variations of the applied mechanical vibration amplitude and frequency.

When the vibration amplitude was increased further, the frequency was increased gradually. Then, the flow transitions from periodic to quasi-periodic oscillation flow with incommensurate frequencies. After this, the quasi-periodic oscillation is destroyed by increasing the vibration amplitude value, and maybe chaotic flow oscillation appears. For the limited computer performance, this work did not consider the amplitude of vibration greater than 100 mm for chaotic flow at frequency 1 Hz and time 900 sec.

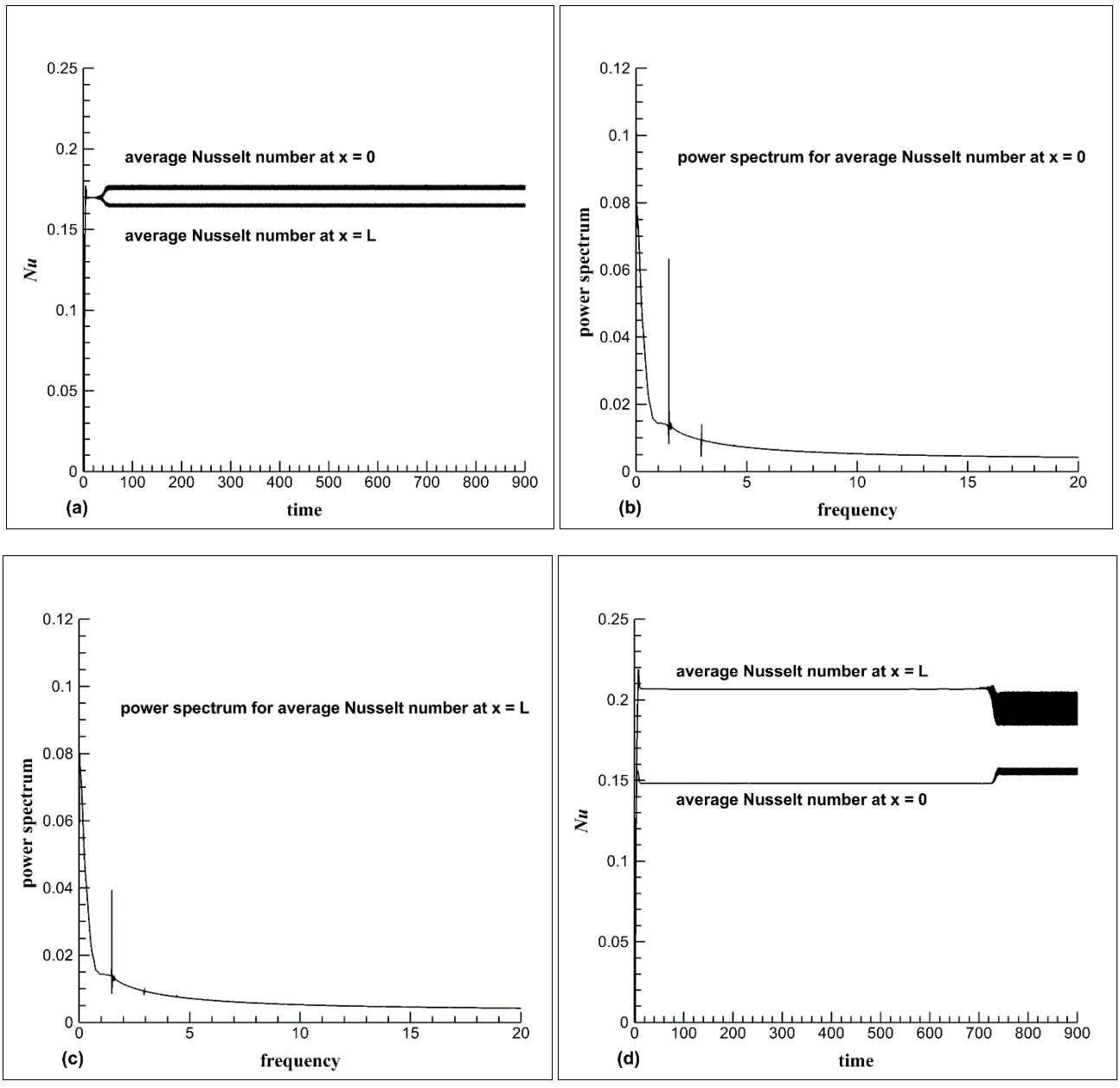

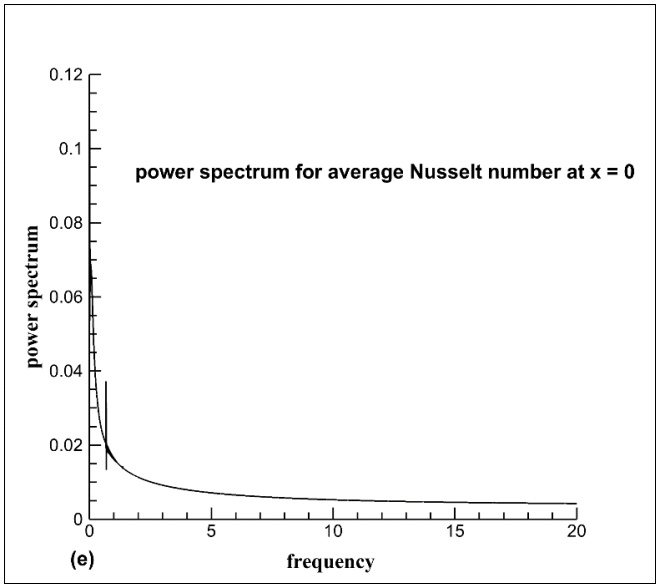
power spectrum for average Nusselt number at x = 0
power spectrum
frequency
(e)

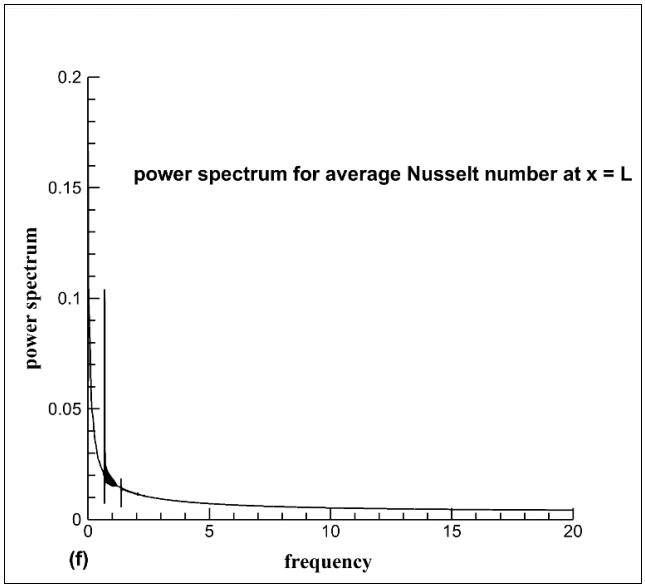
power spectrum for average Nusselt number at x = L
power spectrum
frequency
(f)

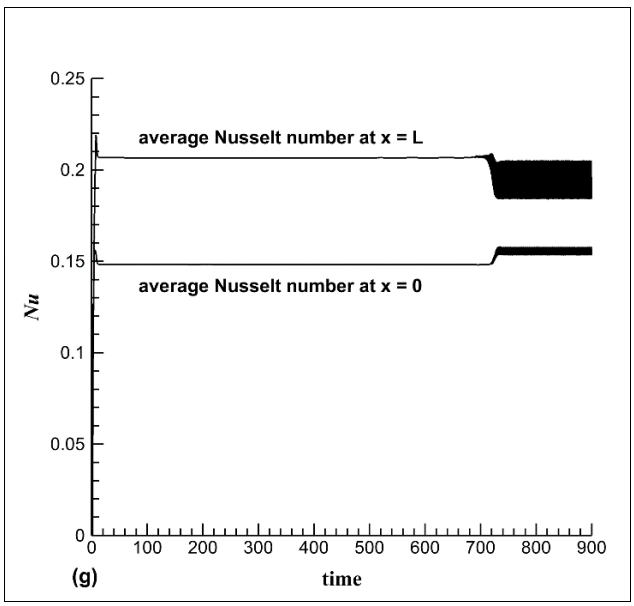
average Nusselt number at x = L
average Nusselt number at x = 0
Nu
time
(g)

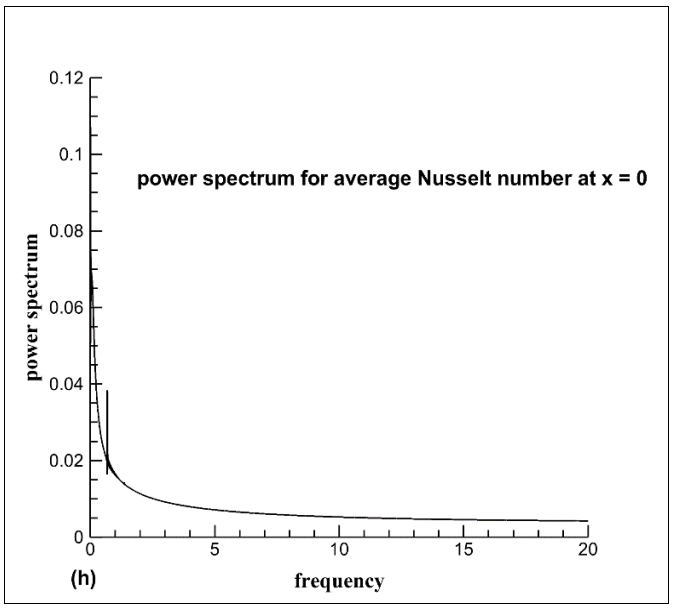
power spectrum for average Nusselt number at x = 0
power spectrum
frequency
(h)

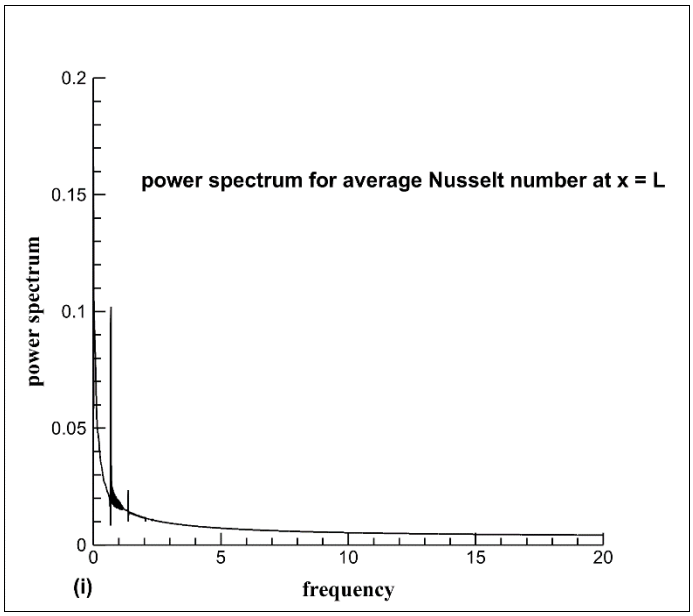
power spectrum for average Nusselt number at x = L
power spectrum
frequency
(i)

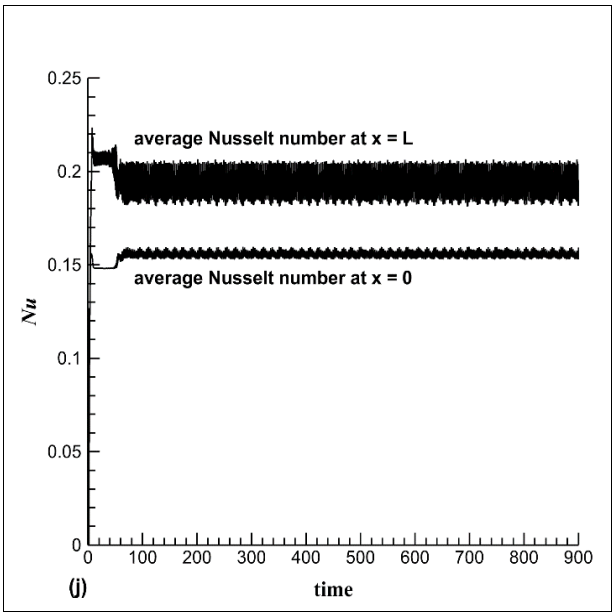
average Nusselt number at x = L
average Nusselt number at x = 0
Nu
time
(j)

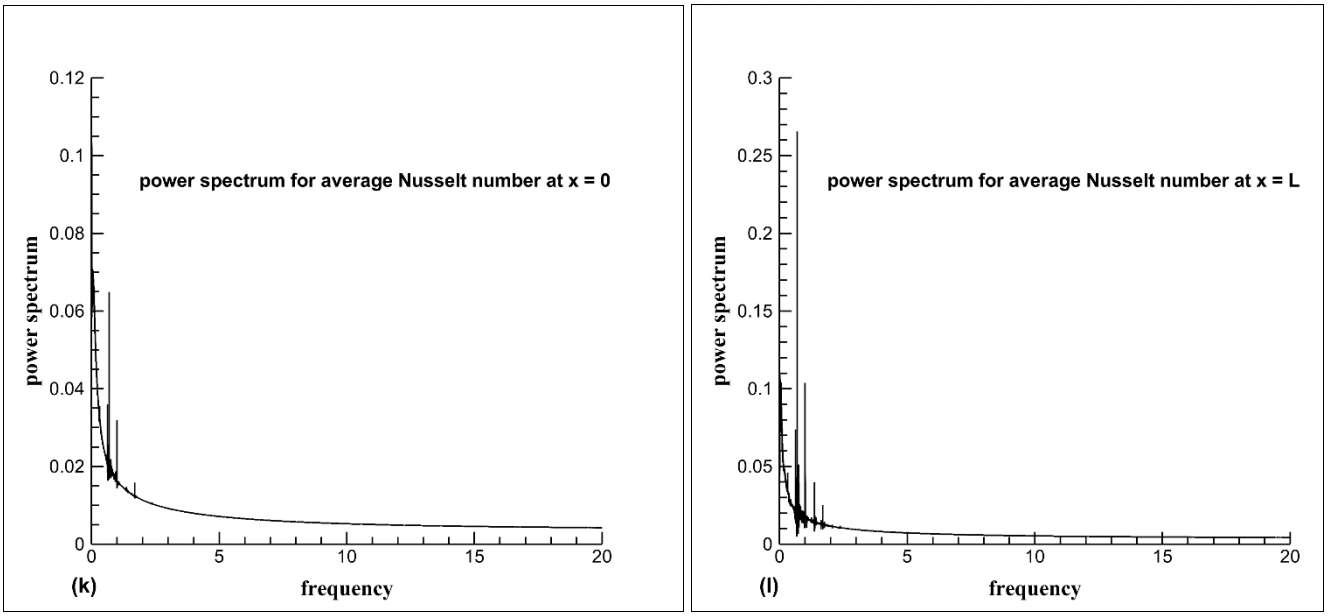

Fig 6: Time series of average Nusselt number (left) oscillations and power spectrum for average Nusselt number at $x = 0$ and L (right) without and with thermovibration effect for $Pr = 0.024$, $Ra_I = 10^6$ and $t = 900$ sec, thermovibration starts at $t = 0$ sec and stops at $t = 900$ sec: (a, b, c) without thermovibration effect; (d, e, f) with thermovibration effect at $f = 1$ Hz and $b = 0.01$ mm; (g, h, i) with thermovibration effect at $f = 1$ Hz and $b = 1.0$ mm; (j, k, l) with thermovibration effect at $f = 1$ Hz and $b = 100$ mm.

The time evolution of heat transfer rate and frequency power spectrum of average Nusselt number analysis was illustrated in Fig. 6. It can be noted, that without the application of vibration as shown in Fig. 6(a), the average Nusselt number oscillates periodically with fundamental frequency is 1.425 Hz and double frequency is 2.922 Hz at $x = 0$ and L as shown in Fig. 6(b) and (c), respectively.

While with vibration and at frequency $f = 1$ Hz and amplitude $b = 0.01$ mm the average Nusselt number is periodic as shown in Fig. 6(d). A fundamental frequency is 0.69 Hz appears at $x = 0$ as shown in Fig. 6(e), and a fundamental frequency is 0.69 Hz with a double fundamental frequency is 1.35 Hz appears at $x = L$ as shown in Fig. 6(f). When the vibration amplitude is increased to $b = 1.0$ mm at frequency $f = 1$ Hz the average Nusselt number is periodic as shown in Fig. 6(g). A fundamental frequency is 0.68 Hz appears at $x = 0$ as shown in Fig. 6(h) and a fundamental frequency is 0.68 Hz with a double fundamental frequency is 1.36 Hz appears at $x = L$ as shown in Fig. 6(i). As the vibration amplitude increased further to $b = 100$ mm at frequency $f = 1$ Hz the periodic oscillation average Nusselt number evolved into a quasi-periodic oscillation average Nusselt number as shown in Fig. 6(j). During the quasi-periodic mode, the heat transfer rate oscillation with four incommensurate frequencies: 0.6244 Hz, 0.68 Hz, 0.9638 Hz, and 1.6825 Hz at $x = 0$ as shown in Fig. 6(k) and with five incommensurate frequencies: 0.6216 Hz, 0.68 Hz, 0.7414 Hz, 1.0 Hz and 1.37 Hz at $x = L$ as shown in Fig. 6(l).

To observe the quantitatively natural convection flows and to describe the heat transfer through the enclosure, the local Nusselt number distribution along the vertical cooled walls was plotted in Fig. 7 for different vibration amplitude values and at a certain vibration frequency of $f = 1$ Hz. The mechanical vibrational has more effect on the heat transfer coefficient in all cases compared with the non-vibrated case. As a consequence, the heat transfer through the cold walls is notably enhanced at the lower half of the cold walls, but it is reduced at the upper half of the cold walls.

4.2. The effect of nonuniform vibration amplitude at a constant vibration frequency

This section is devoted to studying the effect of nonuniform vibration amplitude by taking two different values of amplitude 50 mm and 100 mm, which are effective in a sequential pattern on an enclosure at a constant vibration frequency of 1 Hz. In another meaning and for clarification, after the thermal flow starts and when time becomes $t = 30$ sec then the vibration applying at amplitude 50 mm to the time becomes $t = 45$ sec, and when the time becomes $t > 45$ sec the vibration applying at amplitude 100 mm to the time become $t = 60$ sec, and vice versa. However, at the time becomes $t > 60$ sec the applied vibration will be cancelled.

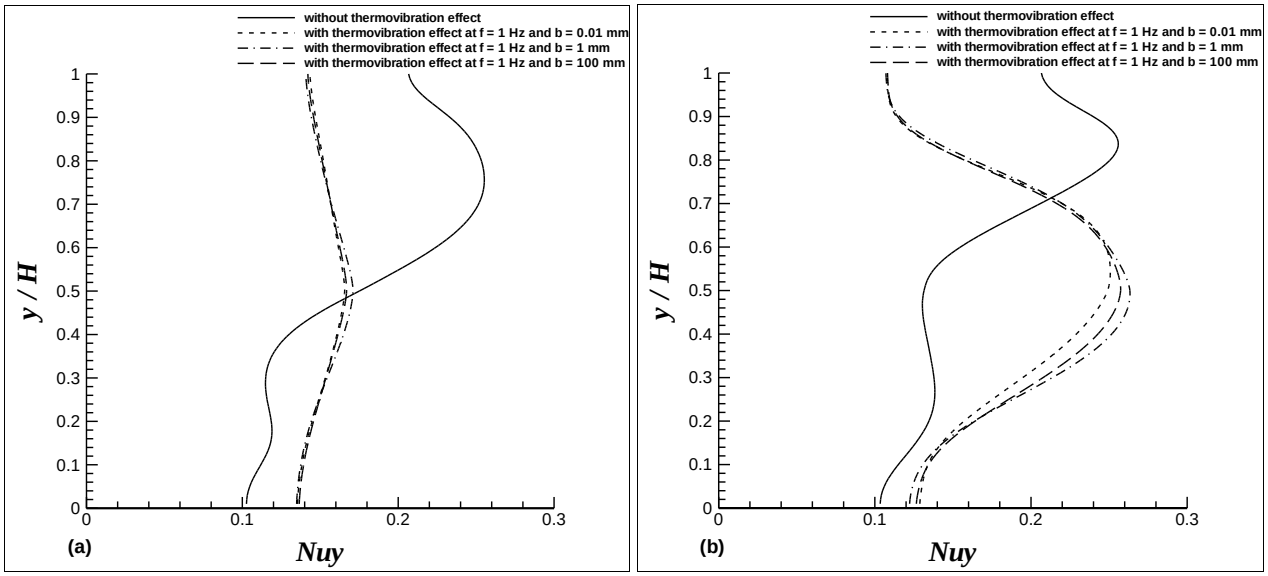

Fig 7: Local Nusselt number distribution along the vertical walls without and with thermovibration effect for Pr = 0.024, Ra_I = 10^6 and t = 900 sec. Thermovibration starts at t = 0 sec and stops at t = 900 sec: (a) at x = 0; (b) x = L.

Initially when only static gravity exists and without the effect of vibration, the fluid is at rest with low-temperature T_c. Then, the fluid is subjected to high temperature due to internal heat generating, thus the fluid in the enclosure is driven by buoyancy force due to gravity. The flow patterns consist of two primary convective vortices rotating in opposite directions with approximately equal strength. The two vortices become asymmetric with different sizes and the small secondary vortex is present in the lower corner for the right side of the enclosure it is rotating in the clockwise direction, thus the natural periodic oscillation flow is being observed. The thermal flow and isotherms at time 90 sec are illustrated in Fig. 8(a) and (b). The thermal flow and temperature distribution in an enclosure, at the time t = 90 sec with the vibration applied in the sequential pattern at amplitude 50 mm and 100 mm with frequency f = 1 Hz are shown in Fig. 8(c) and (d), respectively. The thermal flow vortex is settled into a spatially asymmetric; the fluid rises along the center region of the enclosure and then circulates toward the cold walls along which it falls and circulates toward the center region of the enclosure. When vibration is applied in a sequential pattern at amplitude 100 mm and 50 mm with frequency f = 1 Hz, the thermal flow fields are represented by multicellular and three-cell structures. The maximum magnitude of the streamfunction is occur at the vortex core where it is magnitude decreases away from the vortex core as illustrated in Fig. 8(e) and the instantaneous temperature distribution field shown in Fig. 8(f). The change of the sequence arrangement for the two different values of amplitude is 50 mm and 100 mm in a time series, which affects the thermal flow in the enclosure and causes thermal flow transition from a two-cell dominating structure as shown in Fig. 8(c), to three-cell dominating structure as shown in Fig. 8(e). The thermal flow in an enclosure is a time-dependent flow, hence any change in vibration amplitude leads to the flow becoming unstable and vortices forming or disappearing.

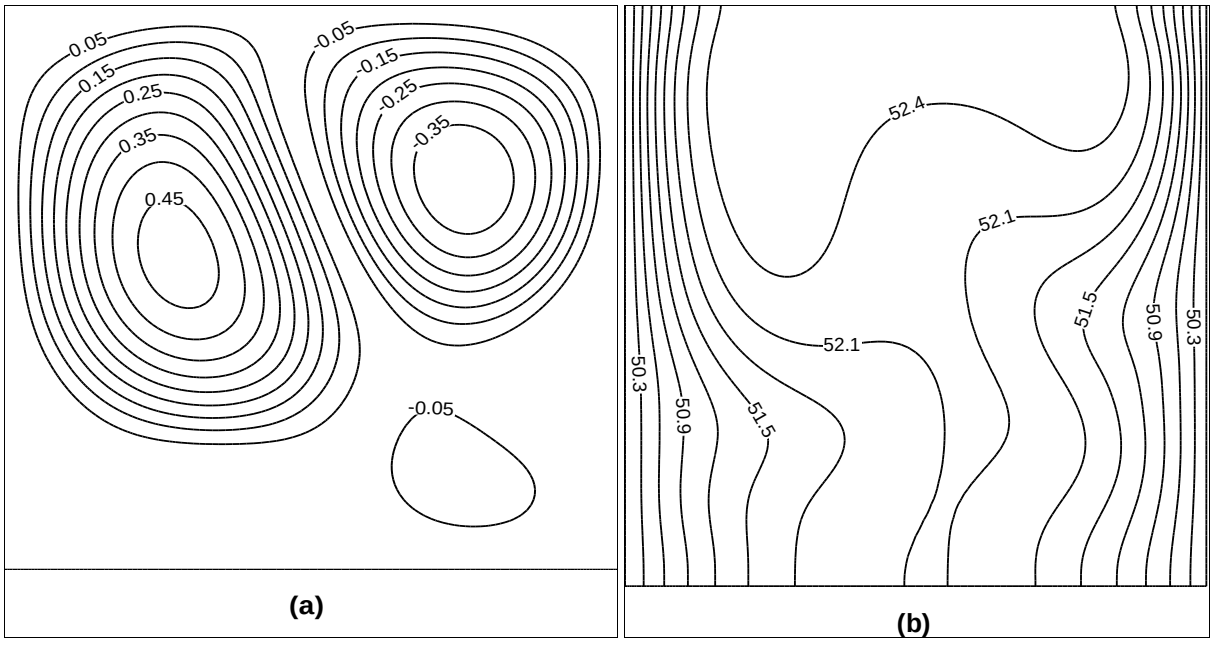

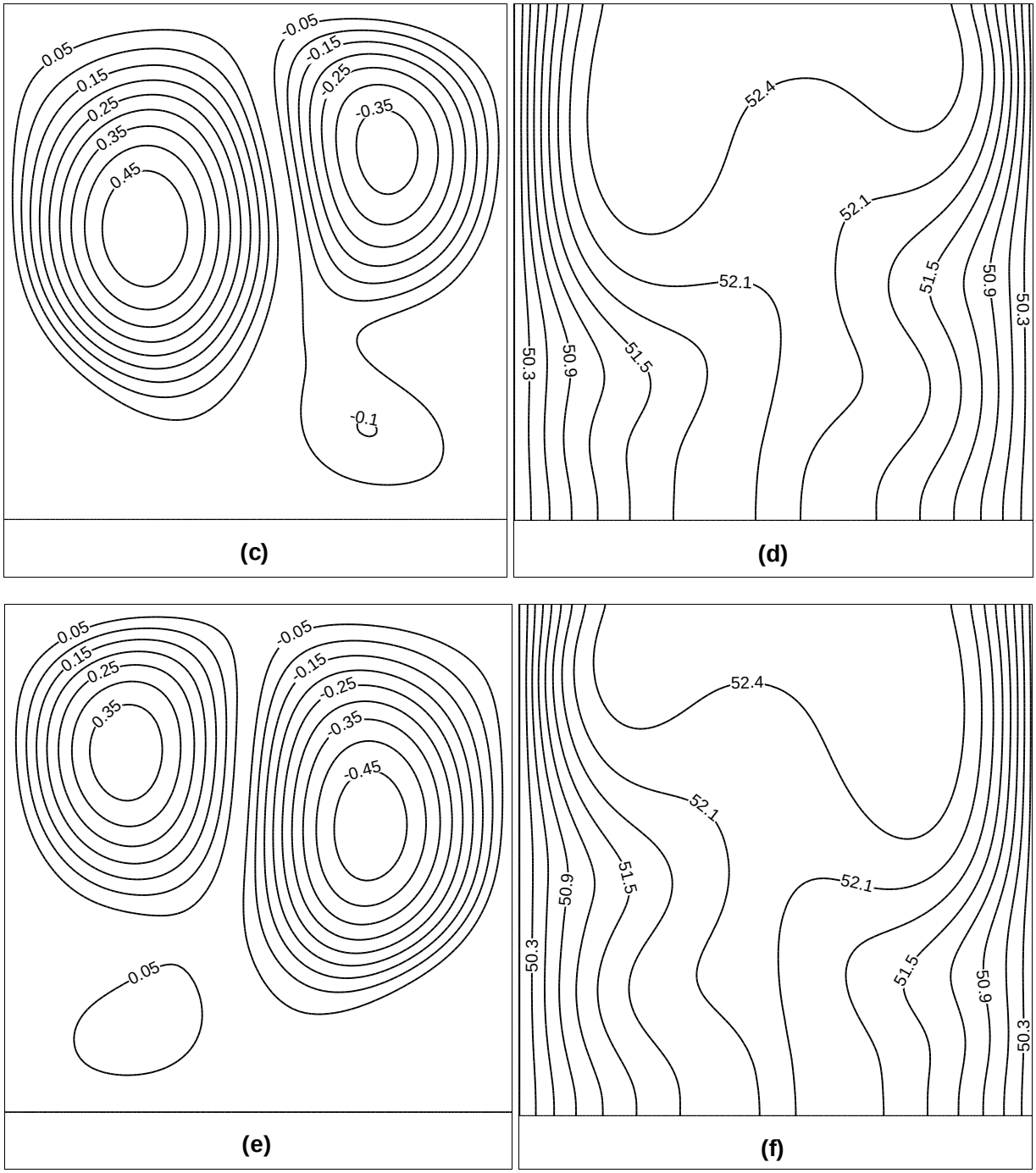

Fig 8: Streamfunctions (left) and Isotherms (right) without and with thermovibration effect for Pr = 0.024, Ra_I = 10^6 and t = 90 sec. Thermovibration for f = 1 Hz starts at t = 30 sec and stops at t = 60 sec: (a, b) without thermovibration effect; (c, d) at 30 sec ≤ t ≤ 45 sec with b = 50 mm and at 45 sec < t ≤ 60 sec with b = 100 mm; (e, f) at 30 sec ≤ t ≤ 45 sec with b = 100 mm and at 45 sec < t ≤ 60 sec with b = 50 mm.

The oscillatory of maximum and minimum streamfunction versus time when the vibration is applied at sequential pattern effect of two different values of amplitude 50 mm and 100 mm with frequency f = 1 Hz was illustrated in Fig. 9(a). At time becomes t = 30 sec the applied vibration amplitude is 50 mm, because of this, a rapid decrease in maximum streamfunction value to become 0.047 m^2/sec at time t = 34.588 sec and rapid increases in minimum streamfunction value to become - 0.681 m^2/sec at time t = 33.15 sec. The reason for this is that the clockwise streamfunction which widening at the expense of the counterclockwise streamfunction. The motion of the fluid becomes unstable and oscillation is non-periodic for maximum streamfunction and disappearing oscillation phenomenon for minimum streamfunction as plotted in Fig. 9(a). While at the time becomes t > 45 sec the applied vibration amplitude is 100 mm, and the flow is non-repeating, irregular, and chaotic. At the time becomes t > 60 sec the applied vibration is cancelled and for this a sudden increase in maximum streamfunction value to become 0.555 m^2/sec at time t = 63.105 sec and a sudden decrease in minimum streamfunction value to become - 0.280 m^2/sec at time t = 63.105 sec. this is due to the counterclockwise streamfunction, which is widening at the expense of the clockwise streamfunction. Finally, the thermal flow becomes a natural periodic oscillation flow at values equal to the values without the external mechanical vibration effect. The oscillation trajectory which related to the

velocity components u and v at the point (3/5, 3/5), which are plotting both quantities as phase variables over a significant length of time as shown in Fig. 9(b). For this case, the oscillation trajectory encompasses three main regions; the first region describes the flow at 23.55 sec $\leq t \leq$ 30 sec where the flow starts to oscillate. The second region describes the flow at 33.1 sec $\leq t \leq$ 60.4 sec where the mechanical vibration was applied in the sequential pattern at amplitude 50 mm and 100 mm with frequency f = 1 Hz which encompasses an even larger u - v area due to the motion becoming irregular oscillation. The third region describes the flow at 65.61 sec $\leq t \leq$ 90 sec where the applied mechanical vibration was cancelled, and flow transitioned to periodic oscillation flow.

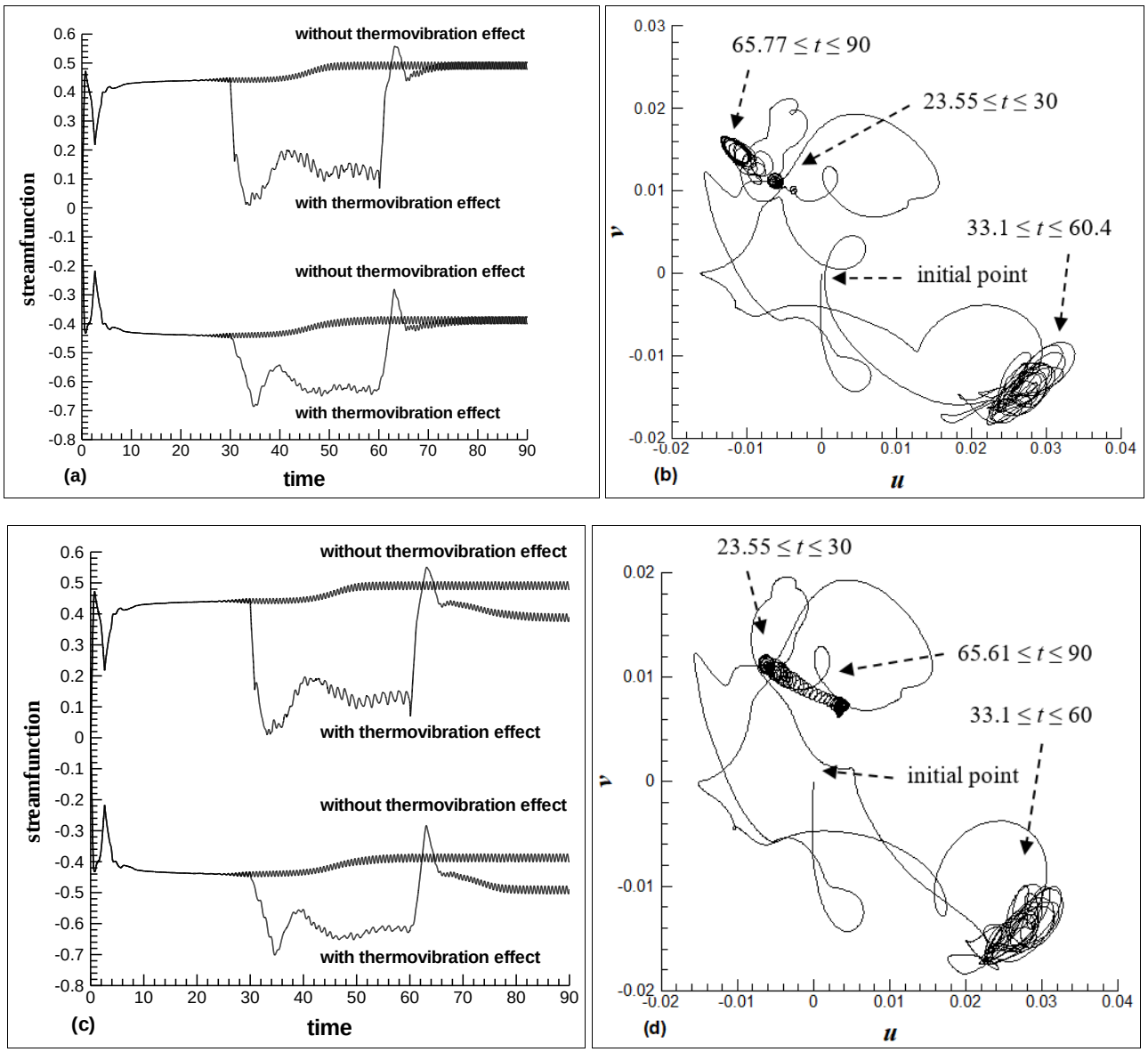

Fig 9: Time series of maximum (> 0) and minimum (< 0) streamfunction (left) oscillations without and with thermovibration effect for Pr = 0.024, $Ra_I = 10^6$ and t = 90 sec and oscillation trajectory for u-velocity and v-velocity at x = 3/5 L and y = 3/5 H with thermovibration effect (right). Thermovibration for f = 1 Hz starts at t = 30 sec and stops at t = 60 sec: (a, b) at 30 sec $\leq t \leq$ 45 sec with b = 50 mm and at 45 sec < t ≤ 60 sec with b = 100 mm; (c, d) at 30 sec $\leq t \leq$ 45 sec with b = 100 mm and at 45 sec < $t \leq$ 60 sec with b = 50 mm.

Fig. 9(c) illustrates the oscillation of maximum and minimum streamfunction versus time when the vibration is applied in a sequential pattern of two different values of amplitude 100 mm and 50 mm at a frequency of 1 Hz. When time becomes t = 30 sec, the external mechanical vibration is applied at an amplitude of 100 mm. Therefore, a sudden decrease in maximum streamfunction value to 0.012 m^2/sec at time t = 33.23 sec which is lesser than the value of maximum streamfunction shown in Fig. 9(a), and a sudden increase in minimum streamfunction value to -0.701 m^2/sec at time t = 34.58 sec. The flow becomes oscillation irregular and non-periodic. When the time is t = 45 sec the amplitude is 50 mm was applied and the flow for maximum and minimum streamfunction becomes quasi-periodic. The external mechanical vibration is cancelled at the time becomes t = 60 sec so a sudden increase and decrease in maximum and minimum streamfunction value to 0.551 m^2/sec and -0.286 m^2/sec, respectively, at time t = 63.18 sec. The flow becomes unstable and then returns to natural periodic oscillation with values that differ from the values of streamfunction without any influence by vibration, see Fig. 8(a). The oscillation trajectory for this case is shown in Fig. 9(d) and it encompasses three significant oscillation regions; the first region describes the flow at 23.55 sec $\leq t \leq$ 30 sec,

where the flow transitions from unstable to oscillation. The second region describes the flow at 33.1 sec $\leq t \leq$ 60 sec where the mechanical vibration is applied. The third region describes the flow at 65.61 sec $\leq t \leq$ 90 sec where the application of mechanical vibration was canceled and flow transitioned to natural periodic oscillation flow.

A time history of average Nusselt number and power spectra is illustrated in Fig. 10. At without vibration effect the average Nusselt number oscillates periodically as shown in Fig. 10(a), with a fundamental frequency is 1.47 Hz at $x = 0$ and L as plotted in Fig. 10(b) and (c), respectively.

At application of vibration with frequency 1 Hz and amplitude 50 mm and then 100 mm, the average Nusselt number transitions from periodic state to non-periodic state at the amplitude of vibration is 50 mm and then transitions to chaotic state at the amplitude of vibration is 100 mm. Finally, the average Nusselt number is returned to the natural periodic oscillation state after the vibration is canceled as shown in Fig. 10(d). Therefore, the numbers of frequencies have appeared in the power spectrum at $x = 0$ and L as illustrated in Figs. 10(e) and (f). This state also is shown at the application of vibration with a frequency of 1 Hz and amplitude of 100 mm and then 50 mm, as shown in Fig. 10(g). The average Nusselt number transition from a periodic state to a non-periodic state at the amplitude of vibration is 100 mm and then transitions to a quasi-periodic state at the amplitude of vibration is 50 mm and after the vibration is cancelled the average Nusselt number returns to natural periodic oscillation. The power spectrum for the average Nusselt number is plotted in Fig. 10(h) and (i).

The heat transfer through the vertical of two cooled walls is represented by local Nusselt number distribution as plotted in Fig. 11. The maximum local Nusselt number value is located on the right cold wall of the enclosure at $x = L$ and $y/H = 0.83$ when the vibration is applied in sequential pattern with amplitude 50 mm and then 100 mm. However, the vibration in a sequential pattern with an amplitude of 100 mm and then 50 mm, is located on the left cold wall of the enclosure at $x = 0$ and $y/H = 0.83$. This is due to the vortex causing the boundary layer to be stable and thin.

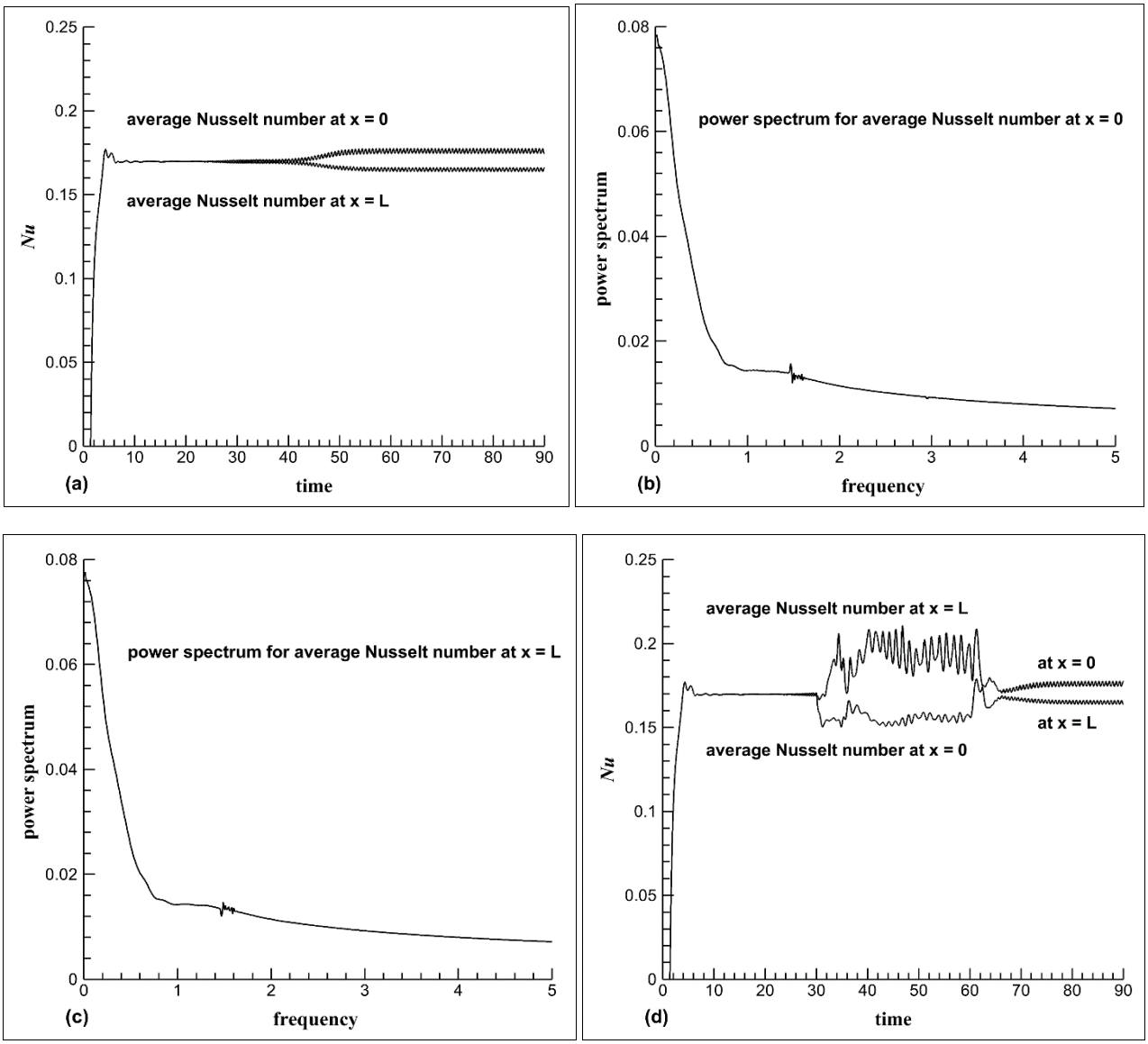

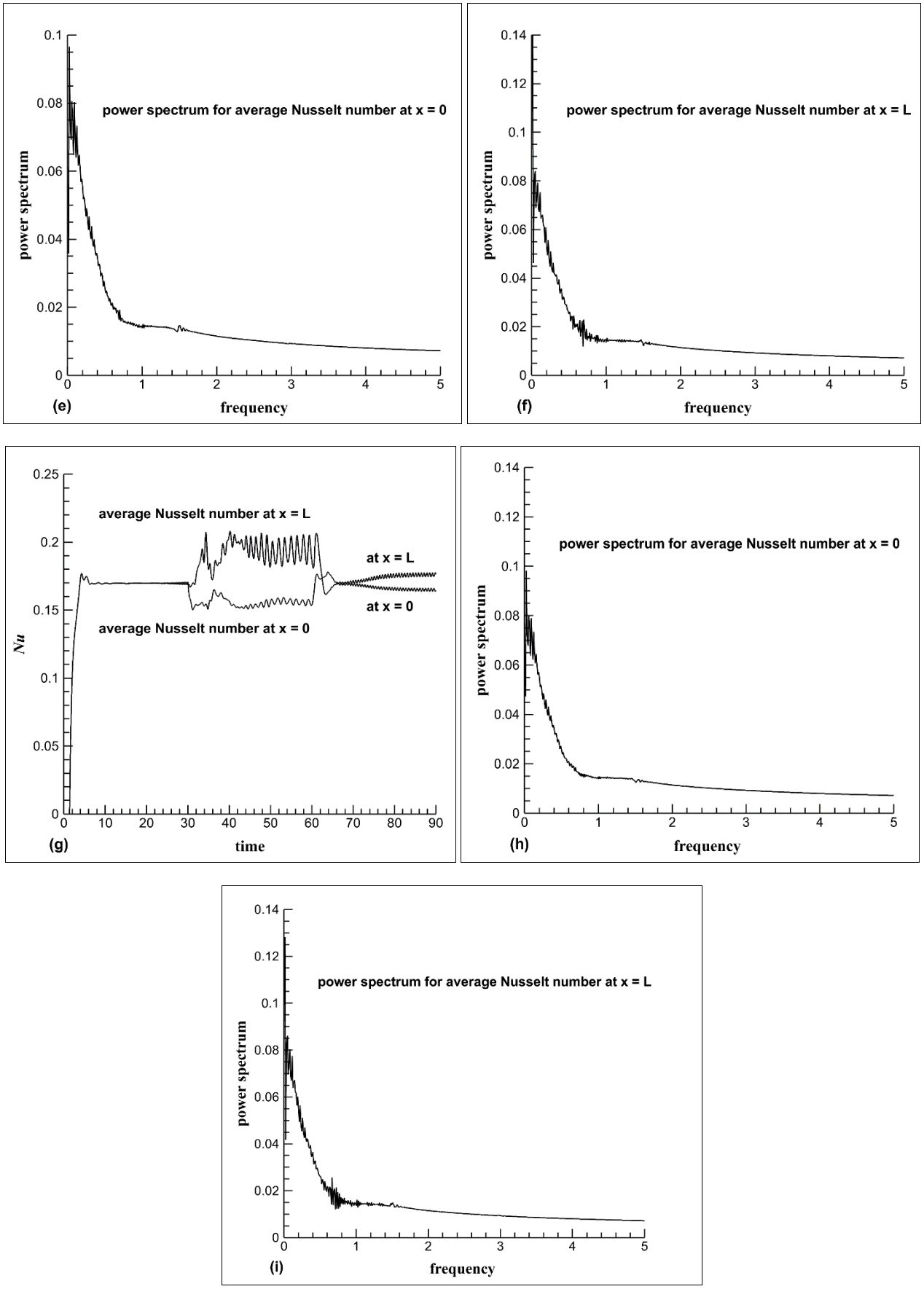

Fig 10: Time series of average Nusselt number (left) oscillations and power spectrum for average Nusselt number at $x = 0$ and L (right) without and with thermovibration effect for $Pr = 0.024$, $Ra_I = 10^6$ and $t = 90$ sec, thermovibration for $f = 1$ Hz starts at $t = 30$ sec and stops at $t = 60$ sec: (a, b, c) without thermovibration effect; (d, e, f) with thermovibration effect for 30 sec $\leq t \leq$ 45 sec at $b = 50$ mm and for 45 sec $< t \leq 60$ sec at $b = 100$ mm; (g, h, i) with thermovibration effect for 30 sec $\leq t \leq$ 45 sec at b = 100 mm and at 45 sec $< t \leq 60$ sec at $b = 50$ mm.

In this study, someone can see that the natural periodic oscillation flow makes the vortices spatially asymmetric and have unequal strength but any influence of external mechanical vibration at a certain frequency and amplitude generates the new vortices, which are spatially asymmetric and have unequal strength. Thus, the external mechanical vibration causes a distorted natural periodic oscillation flow phenomenon, so another oscillation appears at a certain frequency and amplitude with the appearance of a different pattern of flow. The amplitude and frequency of the thermal fluid flow are dependent on the combined effect of the external mechanical vibration applied and the buoyancy force generated by gravity.

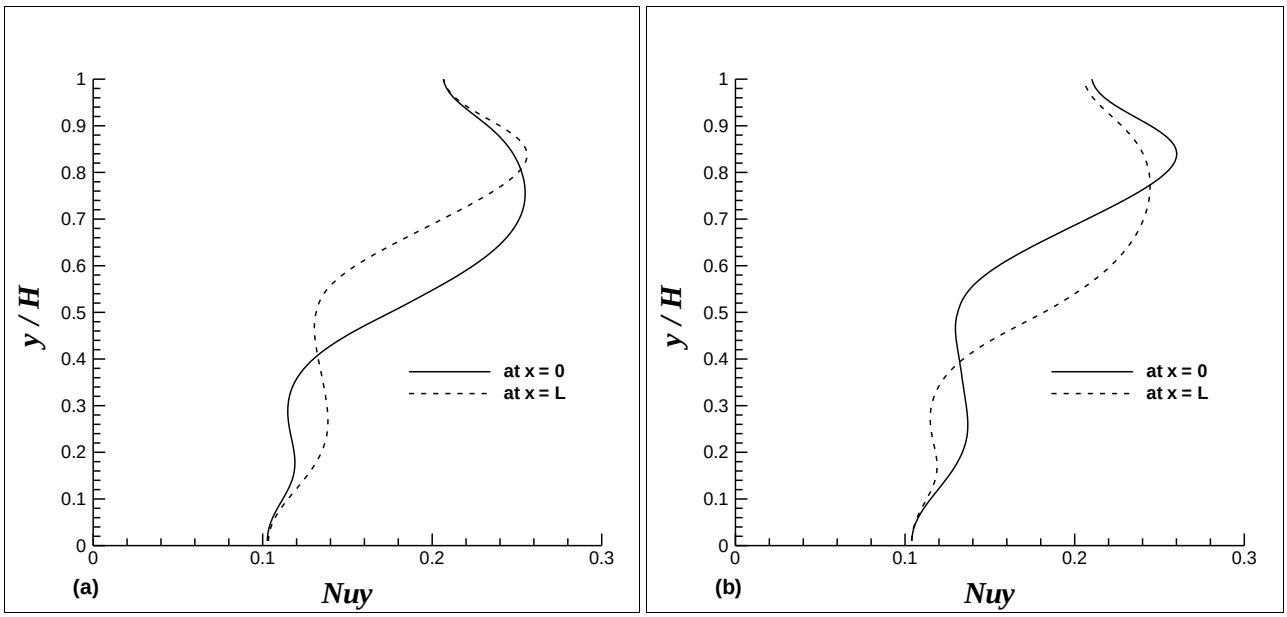

Fig 11: Local Nusselt number distribution along the vertical walls with thermovibration effect for $Pr = 0.024$, $Ra_l = 10^6$ and $t = 900$ sec. Thermovibration for $f = 1$ Hz starts at $t = 30$ sec and stops at $t = 60$ sec: (a) at 30 sec $\leq t \leq$ 45 sec with $b = 50$ mm and at 45 sec $< t \leq 60$ sec with $b = 100$ mm; (b) at 30 sec $\leq t \leq 45$ sec with $b = 100$ mm and at 45 sec $< t \leq 60$ sec with $b = 50$ mm.

5. Conclusion

Numerical investigation of periodic oscillation natural convection inside internally uniform heated square enclosure subject to a sinusoidal oscillation vibration. The vibration was applied parallel to the direction of gravity acceleration. The top and bottom walls of the two-dimensional enclosure were isolated, whereas the side walls were isothermal cooled. The enclosure was filled by molten gallium with Prandtl number 0.024 as liquid metal and internal Rayleigh number 10^6. A time-dependent governing equation was solved by using a finite volume method based on a pressure-correction equation of the unsteady SIMPLE algorithm technique, and a collocated arrangement for scalar and vector variables in a non-uniform grid system.

From the time history of streamfunctions, it can be observed that the vibration at a certain value of frequency and uniform amplitude can be eliminated from the natural periodic oscillation flow and the thermal flow becomes non-oscillation. Furthermore, after a significant length of time and at the effect of the same vibration frequency and amplitude value a sudden unexpected change in flow pattern occurs where the thermal flow becomes oscillation. It means the vibration makes the thermal flow unstable and causes fluid vortices to disappear, after a while, it could be returned and repeated. Hence the vibration changes the fluid stability continuously and the thermal flow pattern and temperature distribution. When the vibration amplitude was increased further at the same frequency, the number of frequencies for thermal flow was increased gradually. Then, the flow transitions from periodic to quasi-periodic oscillation with incommensurate frequencies. After that, the quasi-periodic oscillation for thermal flow is destroyed by increasing the vibration amplitude value, and maybe chaotic flow oscillation appears.

It is also seen that when the flow transitions from unsteady to natural periodic oscillation, and the vibration is applied with two different amplitude values (nonuniform effect) in a sequential pattern at a certain frequency value, the thermal flow becomes unstable. This caused a sudden change in the sizes and strengths of vortices and a new oscillation pattern flow appeared. When the vibration effect is cancelled, a thermal flow returns to natural periodic oscillation phenomena but with streamfunctions values dependent on vibration amplitude values that were effective at a certain frequency value. This means the effect of the vibration continues for some time even after it is cancelled.

The results have also demonstrated that the average Nusselt number is proportional to vibration frequency and amplitude. Moreover, the external mechanical vibration can enhance or reduce the heat transfer rate of thermal flow in the enclosure. Thus, the variation of the average Nusselt number decreases at the left wall and increases at the right wall with changing vibration amplitudes or frequency values. This means that the heat transfer to the left wall is unequal to the heat transfer to the right wall. Finally, the local Nusselt number along the two cooled walls shows that the heat transfer rate enhanced at the lower half of the cold walls, but reduced at the upper half of the cold walls.

The effect of vibration must be studied for unsteady thermal flow over a significant length of time because it has an unexpected effect on the natural periodic oscillation flow, it is difficult to notice it is an effect in a short length of time.

Nomenclature

b	Amplitude (m)
Cp	Specific heat at constant pressure (J/kg K)
f	Frequency (Hz)
g	Acceleration due to gravity (m/sec^2)
H	Enclosure height (m)
L	Enclosure width (m)
k	Thermal conductivity (W/m K)
Nu	Average Nusselt number
Nu_y	Local Nusselt number
p	Pressure (N/m^2)
Q	Internal volumetric heat generation (W/m^3)
Pr	Prandtl number, ν / α
Ra_I	Internal Rayleigh number, $g \beta QL^5 / \alpha \nu k$
T	Temperature (K)
T_c	Cold wall temperature (K)
T_{max}	Maximum fluid temperature (K)
T	Time (sec)
U	Velocity of x-component (m/sec)
V	Velocity of y-component (m/sec)
x, y	Cartesian co-ordinates (m)
Greek letters	
α	Thermal diffusivity (m^2/sec)
β	Volumetric coefficient of expansion (K^{-1})
μ	Dynamic viscosity of fluid (kg/m sec)
ν	Kinematics viscosity of fluid (m^2/sec)
ρ	Density of fluid (kg/m^3)
ω	Angular frequency (rad/sec^2)
ψ	Streamfunction (m^2/sec)

References

1. Praneeth MN, Anees MI, Ashwin S, Sandesh B, Ramis MK. Numerical investigation on heat transfer characteristics of a nuclear fuel rod. In: 2010 International Conference on Mechanical and Electrical Technology; 2010 Sep 10-12; Singapore. p. 239-244. DOI: 10.1109/ICMET.2010.5598358.
2. Pandey KM, Mahesh M. Determination of temperature distribution in a cylindrical nuclear fuel rod - a mathematical approach. International Journal of Innovation, Management and Technology. 2010 Dec;1(5):464-468. DOI: 10.7763/IJIMT.2010.V1.81.
3. Mesquita AZ, Rezende HC, da Costa ACL. Experimental determination of heat transfer coefficients in uranium zirconium hydride fuel rod. In: 2005 International Nuclear Atlantic Conference; 2005 Aug 28 - Sep 2; Santos, SP, Brazil.
4. Dinesh PA, Nalinakshi N, Chandrashekhar DV. Effect of internal heat generation and variable fluid properties on mixed convection past a vertical heated plate. Fluid Dynamics and Materials Processing. 2014 Jan;10(4):465-90. DOI: 10.3970/fdmp.2014.010.465.
5. Zhukov AV, Kuzina JA, Uhov VA, Sorokin GA. Natural convection as the way of heat removal from fast reactor core at cool down regime. Available from: https://inis.iaea.org/collection/NCLCollectionStore/_Public/31/032/31032893.pdf
6. Abdillah H, Saputra G, Novitrian, Permana S. Study of natural convection passive cooling system for nuclear reactors. Journal of Physics: Conference Series. 2017 Jul;877:012047. DOI: 10.1088/1742-6596/877/1/012047.
7. Chacha H, Saghir MZ. Solutal-thermo-diffusion convection in a vibrating rectangular cavity. International Journal of Thermal Science. 2005 Jan;44(1):1-10. DOI: 10.1016/j.ijthermalsci.2004.04.013.
8. Lan CW. Effect of axial vibration on vertical zone-melting processing. International Journal of Heat and Mass Transfer. 2000 Jun;43(11):1987-1997. DOI: 10.1016/S0017-9310(99)00264-1.
9. Kim SK, Kim SY, Choi YD. Resonance of natural convection in a side heated enclosure with a mechanically oscillating bottom wall. International Journal of Heat and Mass Transfer. 2002 Jul;45(15):3155-3162. DOI: 10.1016/S0017-9310(02)00030-3.
10. Mahmud S, Fraser RA. Vibrational effect on entropy generation in a square porous cavity. Entropy. 2003 Dec;5(5):366-76. DOI: 10.3390/e5050366.
11. Jalil JM, Al-Tae'y KA. Themovibrational convection in an enclosure with magnetic field damping. Numerical Heat Transfer, Part A: Applications. 2008 Apr;53(7):766-786. DOI: 10.1080/10407780701715752.
12. Liu QS, Zhou JY, Wing A, Polezhaev VI, Fedyushkin A, Zhou BH, Henri NT, Bernard B. Thermovibrational instability of Rayleigh-Marangoni-Benard convection in two-layer fluid systems. Advances in Space Research. 2008 Dec;41(12):2131-2136. DOI: 10.1016/j.asr.2007.09.016.
13. Shevtsova V, Gaponenko Y, Melnikov D, Ryzhkov I, Mialdun A. Study of thermoconvective flows induced by vibrations in reduced gravity. Acta Astronautica. 2010 Jan-Feb;66(1-2):166-173. DOI: 10.1016/j.actaastro.2009.05.023.
14. Chung S, Vafai K. Vibration induced mixed convection in an open-ended obstructed cavity. International Journal of Heat and Mass Transfer. 2010 Jun;53(13-14):2703-2714. DOI: 10.1016/j.ijheatmasstransfer.2010.02.037.
15. Aktas MK. Thermal convection of a water-based nanofluid in an enclosure with an oscillating wall. In: Proceedings of the World Congress on Engineering; 2011 Jul 6-8; London, U.K. Vol. III.
16. Fedorov OP, Demchenko VF, Shuba IV, Lesnoy AB. Influence of gravitational and vibrational convection on the heat and mass transfer in the melt during crystal growth by the Bridgman and floating zone methods. Inorganic Materials: Applied Research. 2016 May;7(3):437-443. DOI: 10.1134/S2075113316030060.
17. Wang Q, Dai C, Jiao M, Cai Z. Vibration enhanced heat transfer of a hot and a cold microtube with staggered arrangement in an enclosure. In: 1st Asian Conference on Thermal Sciences (ACTS); 2017 Mar 26-30; Jeju Island, Korea.
18. Xie JF, Cao BY. Natural convection of power-law fluids under wall vibrations: A lattice Boltzmann study. Numerical Heat Transfer, Part A: Applications. 2017;72(8):600-627. DOI: 10.1080/10407782.2017.1394134.
19. Crewdson G, Lappa M. The zoo of modes of convection in liquids vibrated along the direction of the temperature gradient. Fluids. 2021;6(30):1-23. DOI: 10.3390/fluids6010030.
20. Al-Tae'y KA, Jaddoa AA, Abd HS, Kadhim RA. A loop thermosyphon for liquid cooled minichannels heat

sink with pulsate surface heat sink. Journal of Thermal Engineering. 2021 May;7(4):1030-1038. DOI: 10.18186/thermal.931389.
21. Chacha M, Saghir MZ. Solutal-thermo-diffusion convection in a vibrating rectangular cavity. International Journal of Thermal Sciences. 2005;44:1-10. DOI: 10.1016/j.ijthermalsci.2004.04.013.
22. Basak T, Roy S, Balakrishnan AR. Effect of thermal boundary conditions on natural convection flows within a square cavity. International Journal of Heat and Mass Transfer. 2006 Nov;49(23-24):4525-4535. DOI: 10.1016/j.ijheatmasstransfer.2006.05.015.
23. Ferziger JH, Perić M. Computational method for fluid dynamics. 3rd rev. ed. Germany: Springer; 2002.
24. Al-Tae'y KA. Natural convection in a laterally and volumetrically heated square enclosure with time-periodic boundary conditions. International Journal of Heat and Technology. 2009 Jan;27(2):77-85.
25. Jalil JM, Al-Tae'y KA, Ismail SJ. MHD natural convection in an enclosure with partially active magnetic field. Numerical Heat Transfer, Part A: Applications. 2013 Jul;64(1):72-91. DOI: 10.1080/10407782.2013.772861.
26. Viskanta R, Kim DM, Gau C. Three-dimensional natural convection heat transfer of a liquid metal in a cavity. International Journal of Heat and Mass Transfer. 1986 Mar;29(3):475-485. DOI: 10.1016/0017-9310(86)90216-4.
27. Tagawa T, Ozoe H. Effect of Prandtl number and computational schemes on the oscillation natural convection in an enclosure. Numerical Heat Transfer, Part A: Applications. 1996 Feb;30(3):271-82. DOI: 10.1080/10407789608913840.
28. Chung JD, Lee JS. Thermal instability during the melting process in an isothermally heated horizontal cylinder. International Journal of Heat and Mass Transfer. 1997 Oct;40(16):3899-3907. DOI: 10.1016/S0017-9310(97)00037-9.
29. Paolucci S, Chenoweth DR. Transition to chaos in a differentially heated vertical cavity. Journal of Fluid Mechanics. 1989 Apr;201:379-410. DOI: 10.1017/S0022112089000984.